QUARTERLY JOURNAL OF THE ROYAL METEOROLOGICAL SOCIETY
Q. J. R. Meteorol. Soc. **00**: 1–21 (2007)
Published online in Wiley InterScience
(www.interscience.wiley.com) DOI: 10.1002/qj.000

Tropical-cyclone intensification and predictability in three dimensions

Nguyen Van Sang[a], Roger K. Smith[a], and *Michael T. Montgomery[b]
[a] *Meteorological Institute, University of Munich, Munich, Germany*
[b] *Dept. of Meteorology, Naval Postgraduate School, Monterey, CA & NOAA's Hurricane Research Division*

Abstract:
We present numerical model experiments to investigate the dynamics of tropical-cyclone amplification and its predictability in three dimensions. For the prototype amplification problem beginning with a weak tropical storm strength vortex, the emergent flow becomes highly asymmetric and dominated by deep convective vortex structures, even though the problem as posed is essentially axisymmetric. The asymmetries that develop are highly sensitive to the boundary-layer moisture distribution. When a small random moisture perturbation is added in the boundary layer at the initial time, the pattern of evolution of the flow asymmetries is dramatically changed and a non-negligible spread in the local and azimuthally-averaged intensity results. We conclude that: 1) the flow on the convective scales exhibits a degree of randomness and only those asymmetric features that survive in an ensemble average of many realizations can be regarded as robust; 2) there is an intrinsic uncertainty in the prediction of maximum intensity using either maximum wind or minimum surface pressure metrics. There are clear implications for the possibility of deterministic forecasts of the mesoscale structure of tropical cyclones, which may have a large impact on the intensity and on rapid intensity changes.
Some other aspects of vortex structure are addressed also: vortex size parameters; sensitivity to the inclusion of different physical processes; and higher spatial resolution. We investigate also the analogous problem on a β-plane, a prototype problem for tropical-cyclone motion. A new perspective on the putative role of the wind-evaporation feedback process for tropical cyclone intensification is offered also here.
The results provide new insight into the fluid dynamics of the intensification process in three dimensions and at the same time suggest limitations of deterministic prediction for the mesoscale structure. Larger-scale characteristics such as the radius of gale force winds, β-gyres, etc. are found to be less variable than their mesoscale counterparts.

KEY WORDS Hurricane; tropical cyclone; typhoon; vortical hot towers, coherent structures, rapid intensification, predictability

Received 23 June 2007; Revised November 18, 2007; Accepted

1 Introduction

There is a growing research literature on the role of asymmetric convection in all phases of tropical-cyclone life cycles with special interest on convectively-induced asymmetries of rainfall and on the effects of various types of asymmetric vortex waves within the hurricane circulation. This research has led to an emerging perspective that many processes occurring within the tropical-cyclone core are manifestations of coherent structures that undergo their own life cycle and may ultimately decay in favor of the symmetric circulation. Studies suggest that asymmetries arise in various ways; many have focussed on the effects of non-trivial vertical wind shear across a developing or mature vortex (e.g., Frank and Ritchie 1999; Reasor *et al.* 2000; Frank and Ritchie 2001; Black *et al.* 2002; Schecter and Montgomery 2003; Reasor *et al.* 2004); and others have examined the structure of vortex-wave asymmetries supported by the vortex itself (Chen and Yau 2001; Chen *et al.* 2003, Wang 2002a, 2002b). The asymmetries can evolve into coherent sub-system-scale vortices that can persist for one or more revolutions about the parent vortex and induce significant intensity changes (e.g., Montgomery *et al.* 2002; Braun *et al.* 2006). Part of the intensity change observed in storms such as Danny (1997) (Blackwell 2000), for example, may be due to the superposition of strong asymmetries, manifest as intense mesovortices, on the symmetric circulation. Supporting evidence comes from the Doppler radar synthesis from Danny as well as earlier studies by, for instance, Marks and Houze (1984). Near cloud-resolving numerical simulations of tropical storm Diana (1984) (Davis and Bosart 2002; Hendricks *et al.* 2004) reveal convectively induced mesovortices. The coherence of these structures is broadly consistent with the idea of "hot towers", proposed almost five decades ago by Riehl and Malkus (1958) to explain the tropical overturning (Hadley) circulation and revived recently to explain hurricane formation, intensification, and evolution as observed in visible and infrared satellite data, lightning data, lidar data and high resolution numerical models (Simpson *et al.* 1998; Montgomery and Enagonio 1998; Möller and Montgomery 2000; Enagonio and Montgomery 2001; Heymsfield *et al.* 2001; Braun

*Correspondence to: Michael T. Montgomery, Dept. of Meteorology, Naval Postgraduate School, Monterey, CA & NOAA's Hurricane Research Division, Miami, FL, USA. Email: mtmontgo@nps.edu

2002; Hendricks *et al.* 2004; Montgomery *et al.* 2006a, hereafter M06). Collectively, the emerging concept is one of intensity and structural change (including warming in the eye) occurring through bursts, fundamentally stochastic in nature, associated with life cycles of asymmetries, rather than though a continuous "slow" evolution connected with the axisymmetric secondary circulation.

The relationship between convectively-induced asymmetries and vertical wind shear has been usefully quantified through the concept of balanced lifting resulting from the presence of a lower-tropospheric vortex in shear. Building on the balanced dynamical interpretations developed by Raymond and Jiang (1990) and Jones (1995), Frank and Ritchie (1999) showed that mesoscale ascent achieved saturation in the lower troposphere and caused a shift of the rainfall from the downshear-right quadrant of the storm to the downshear-left quadrant. Trier *et al.* (2000) and Musgrave *et al.* (2006) have shown that balanced motion within a weak, elevated baroclinic vortex functions in a similar way to focus rainfall and to generate potential vorticity (PV) anomalies. Such anomalies can merge to form a new centre, or a single, dominant anomaly can form a distinct centre and subsume the surrounding vortices. The mesovortices occur over a range of scales from 10 to perhaps 100 km. The smaller ones resemble more the classic hot towers; the larger ones are mesoscale convective vortices, analogous to the cousins from continental convection (Rogers and Fritsch 2001). Larger ones appear capable of forming a new centre; smaller vortices distort and can amplify an existing centre. Importantly, all such vortices share a common property of large cyclonic vorticity in the lower troposphere because of the vigorous organized convection that produced them in an already cyclonic vorticity rich environment. Thus, by vertical vortex-tube stretching near the ocean surface they contribute vorticity to low levels of an existing vortex or can form a low-level circulation by themselves. Either way, the emergent circulation becomes increasingly able to tap the latent reservoir of energy contained in the upper ocean by fluxes of enthalpy across the sea-air interface.

As a first step toward understanding the fluid dynamics of convective bursts and mesoscale vortices in incipient and mature cyclonic storms a mechanism of vortex intensification by vortex Rossby waves (Montgomery and Kallenbach 1997) was proposed and investigated with a range of idealized numerical "thought" experiments that have provided important insights into the influence of convectively-induced potential vorticity (PV) asymmetries on the intensification of tropical storms. Montgomery and Enagonio (1998) and Möller and Montgomery (1999) carried out three-dimensional quasigeostrophic and shallow-water balance-model experiments, respectively, with relatively high wave amplitudes and identified a wave-induced eigenmode that interacts with the tropical-cyclone-like vortex. They hypothesized that the vortex can sustain the eigenmode, which itself can interact with convection and then feed back to the vortex. Subsequent studies by Möller and Montgomery (2000) and Enagonio and Montgomery (2001) confirmed the important role of convectively induced asymmetric flow features in determining the structure and intensity of tropical cyclones. Simple "axisymmetrization" experiments in three dimensions with mono-chromatic azimuthal-wavenumber disturbances and single- and double-cluster PV anomalies show that vortex Rossby waves propagate both radially and vertically. When persistent convection is simulated by adding double-cluster PV anomalies to the PV fields, one after another (so-called "pulsing"), a tropical storm intensifies to hurricane strength with the final intensity dependent on the location and extent of the anomaly. The results support the existence of an alternate means of tropical-cyclone intensification to the axisymmetric mode.

There have been numerous numerical studies of vortex amplification in the prototype problem for tropical-cyclone intensification, which considers the evolution of a prescribed, initially cloud-free, axisymmetric, baroclinic vortex on an f-plane. These studies can be subdivided into those using hydrostatic axisymmetric models with cumulus parameterization (e.g., Ooyama 1969; Emanuel 1989, 1995; Nguyen *et al.* 2002), those using hydrostatic three-dimensional models with cumulus parameterization (e.g., Zhu *et al.* 2001; Zhu and Smith 2002, 2003), and those using hydrostatic three-dimensional models with explicit microphysics (e.g., Wang 2001, 2002a, 2002b), those using non-hydrostatic axisymmetric cloud models (e.g., Willoughby *et al.* 1984; Rotunno and Emanuel 1987; Persing and Montgomery 2003; Hausman *et al.* 2006). There have been many studies also of the analogous flow on a β-plane which is a prototype problem for tropical-cyclone motion (e.g., Kurihara and Tuleya 1990; Flatau *et al.* 1994; Dengler and Reeder 1997; Wang and Holland 1996a, 1996b)[†]. It is significant that non trivial flow asymmetries emerge in all the three-dimensional experiments, even those on the f-plane, and it is our opinion that a fundamental understanding of the intensification process in three-dimensions is still incomplete.

One of the primary goals of the present work is to seek a more complete understanding of the nature of the inner-core asymmetries and their role in tropical-cyclone intensification and motion. To achieve this objective we employ high-resolution numerical experiments using the MM5 model to revisit the prototype intensification problem. In the main suite of numerical experiments we choose the simplest explicit representation of moist processes that mimicks pseudo-adiabatic moist thermodynamics. Using these benchmark experiments we investigate the structure and evolution of the flow asymmetries and their impact on the vortex intensification and motion. A further goal is to investigate the predictability of the vortex intensity and asymmetric flow structure (Lorenz 1969). In contrast with Lorenz (1969), the word "predictability" is used here in qualitative sense to describe the degree of randomness of the ensuing vortex evolution. It is reasonable to expect that

[†]There have been many more studies of this problem in a barotropic context, but our interest here is focussed on baroclinic models with at least three vertical levels to represent the effects of deep convection.

DOI: 10.1002/qj

the asymmetric flow structures are strongly influenced by deep convection, at least in the inner core region, broadly defined as the region with radii less than twice the radius of maximum tangential wind speed at 900 hPa, just above the boundary layer. Since the pattern of deep convection is strongly influenced by the low-level moisture field, which is known to have significant variability on small space scales (e.g. Weckwerth 2000), it is of interest to examine the variability of the inner-core asymmetries as a result of random variations in the boundary-layer moisture distribution. An investigation of this type is the subject of sections 3 and 4.

2 The model configuration

The experiments described below are carried out using a modified version of the Pennsylvania State University-National Center for Atmospheric Research fifth-generation Mesoscale Model (MM5; version 3.6) (Dudhia 1993; Grell *et al.* 1995), which is suitable for the study of idealized problems. The model is configured with three domains: a coarse mesh of 45-km resolution and two, two-way nested domains of 15 and 5 km resolution, respectively. The domains are square and are 5400 km, 1800 km, 600 km on each side. For the experiments on β-plane, the inner-most domain moves to keep the vortex near the centre of the domain. There are 24 σ-levels in the vertical, 7 of which are below 850 hPa. One experiment employing a fourth domain (300x300 km) has been conducted also to permit increased spatial accuracy down to 1.67 km horizontal grid spacing on the inner-most domain.

In order to keep the experiments as simple as possible, the main physics options chosen are the bulk-aerodynamic boundary-layer scheme and the simplest explicit moisture scheme. These schemes are applied in all domains. The sea surface temperature is set to a constant 27^{o}C. The initial vortex is axisymmetric with a maximum tangential wind speed of 15 m s^{-1} at the surface at a radius of 135 km. The strength of the swirling wind decreases sinusoidally with height, vanishing at the top model level (50 hPa). The temperature field is initialized to be in gradient wind balance with the wind field using the method described by Smith (2006). The far-field temperature and humidity are based on Jordan's Caribbean sounding during summertime conditions and are shown in a skew-T log-p diagram in Fig. 1.

Three main sets of experiments are carried out as detailed in Table I and Table II in section 5. The first set, the control set, is performed on an f-plane centred at 20^{0}N and consists of a control experiment and ten additional ones in which the moisture fields throughout the inner-most domain are randomly perturbed at low levels. In the latter, the magnitude of the mixing ratio perturbation lies in the range of (-0.5 g kg^{-1}, 0.5 g kg^{-1}) at levels below 950 hPa. These experiments are carried out using a horizontal grid spacing of 5 km. The second set of experiments differ from the first set only in that they are performed on a β-plane. A third set is conducted on the f-plane in order to: a) assess the impact of evaporative cooling and related

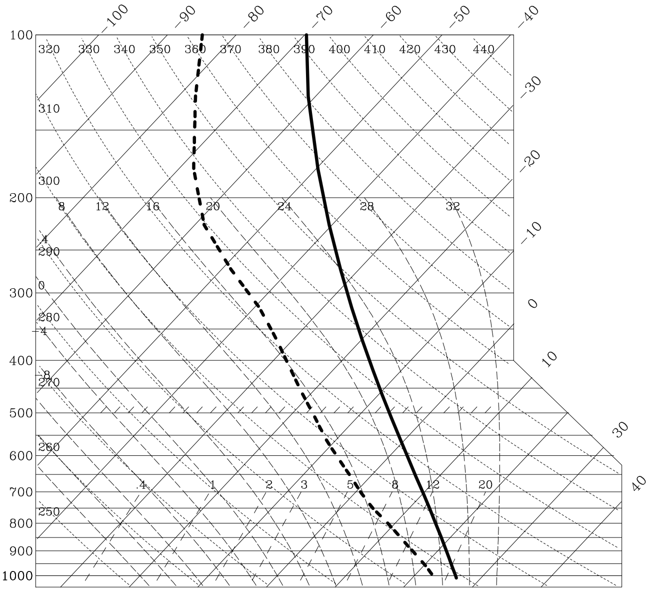

Figure 1. Skew-T log-p diagram showing the temperature (solid line) and dewpoint (dashed line) of the initial sounding at a radius of 2250 km from the domain centre.

downdraft phenomenology on the intensification process simulated in the control set of experiments; b) assess the extent to which a capped wind speed in the sea-to-air enthalpy interaction captures the intensification process in three dimensions; c) assess the robustness of the simulated intensification process to an increased horizontal grid spacing of 1.67 km. The second of these, (b), is informative because it helps discriminate the contribution from the wind-evaporation feedback mechanism of WISHE (an essentially axisymmetric amplification process; Rotunno and Emanuel 1987; Emanuel 1989) and the horizontally localized deep-convection organizational pathway which has *no* axisymmetric counterpart (M06). The integration time for all experiments is 96 h. The results of the three sets of experiments are discussed in section 3, 4, and 5, respectively. In all analyses, the vortex centre is determined by the following procedure. To begin with, a "first-guess" centre is determined by the minimum of the total wind speed at 900 hPa. Then the centre is defined as the centroid of relative vorticity at 900 hPa over a circular region of 200 km radius from the first-guess centre. This method of determining vortex centre shows the least sensitivity to asymmetric features than others (e.g., centre determined by minimum surface pressure), especially during rapid intensification phase when the system is highly asymmetric.

3 Experiments on an f-plane

3.1 Control f-plane experiment

(i) Overview of vortex development

We describe first the development of the initial axisymmetric vortex in the control f-plane experiment (experiment C0 in Table I). Figure 2a shows time-series of

Q. J. R. Meteorol. Soc. **00**: 1–21 (2007)
DOI: 10.1002/qj

Table I. Basic-physics experiments.

No.	Name	Description
C0	Control	Control experiment on an f-plane.
C1-C10	f-plane ensemble	Ten ensemble members. Same as the control experiment, except moisture fields below 950 hPa in domain 3 (5 km) are disturbed by a value in (-0.5 g kg^{-1}, 0.5 g kg^{-1})
B0-B10	β-plane ensemble	Same as C0-C10, except on a β-plane

the minimum surface pressure and maximum total wind speed, VT_{max} at 900 hPa (approximately 1 km high) during a 96 h integration. It shows also the maximum azimuthally-averaged tangential wind speed at 900 hPa, V_{max}, the average being about a centre defined in section 2. As in many previous experiments, the evolution begins with a gestation period during which the vortex slowly decays due to surface friction, but moistens in the boundary layer due to evaporation from the underlying sea surface. This period lasts 9 h during which time the minimum surface pressure rises from its initial value of 1004 hPa to 1008 hPa, but the maximum tangential wind speed decreases only slightly (less than 0.5 m s^{-1}). The imposition of friction from the initial instant leads to inflow in the boundary layer and outflow above it, the outflow accounting for the decrease in tangential wind speed through the conservation of absolute angular momentum. The inflow is moist and as it rises out of the boundary layer and cools, condensation progressively occurs in some grid columns interior to the corresponding radius of maximum tangential wind speed (Smith 1968, Eliassen and Lystad 1977). Existing relative vorticity is stretched and amplified in these columns leading to the formation of localized rotating updrafts. Hendricks *et al.* (2004) and M06 coined the term "vortical hot towers" for these updrafts. As the updrafts develop, there ensues a period lasting about 45 h during which the vortex rapidly intensifies. During this time, V_{max} increases from approximately 14.5 m s^{-1} to approximately 63 m s^{-1} while the minimum surface pressure decreases to 955 hPa. The average intensification rate is approximately 1 m s^{-1} h^{-1}. After 54 h, the vortex attains a quasi-steady state. The minimum surface pressure continues to decline, reaching approximately 945 hPa at 74 h, after which it asymptotes to a slightly smaller value at 96 h. In contrast, V_{max} increases only slightly to approximately 67 m s^{-1} at 96 h, and the swirling wind field in the inner-core region may be regarded as quasi-steady for practical purposes after 54 h. Note that there are large fluctuations in VT_{max}, up to 15 m s^{-1}, during the period of rapid intensification.

In order to determine the cause of the continued decline in the minimum surface pressure during this quasi-steady period, we analyzed the axisymmetric mean geopotential height on the 850 hPa surface (not shown). Since gradient wind balance is an accurate first approximation for the primary circulation above the boundary layer in a mature hurricane, we can use this relationship to determine the relative contribution from the outer core and

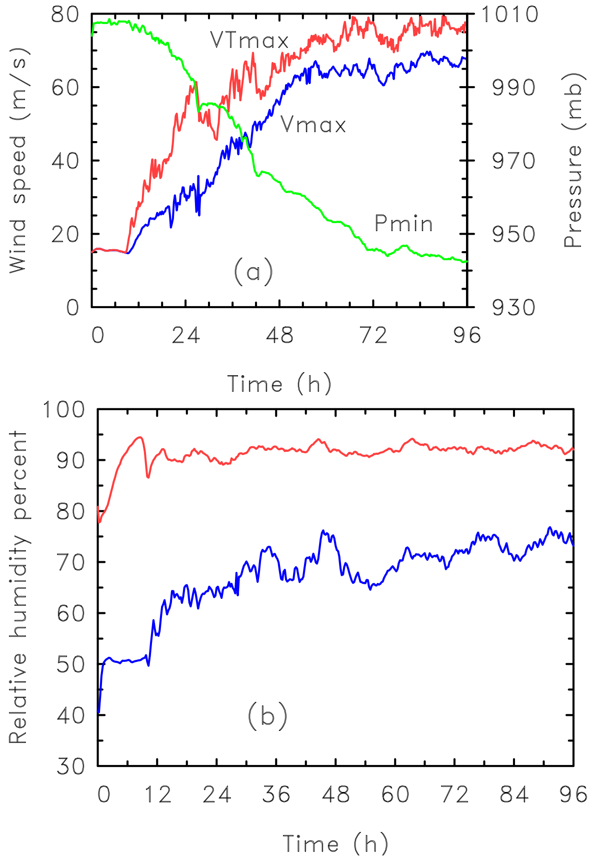

Figure 2. Vortex development in f-plane control experiment (C0). Time-series of: a) Minimum surface pressure (P_{min}), maximum azimuthal-mean (V_{max}) and maximum total wind speed (VT_{max}) at 900 hPa; b) average of relative humidity over a circular region of 100 km radius from vortex centre between 1000 hPa and 900 hPa (upper curve) as well as between 700 hPa and 400 hPa (lower curve).

inner core winds to the minimum geopotential height. It is found that approximately 60% of the drop in geopotential height stems from the wind outside the radius of maximum tangential wind speed (RMW), while the remaining 40% comes from that inside the RMW. It follows then that slightly more than half of the simulated decline in minimum surface pressure after 54 h associated with a strengthening of the outer wind field and the accompanying growth in vortex size.

During the mature stage, the vortex exhibits many realistic features of a mature tropical cyclone, with spiral bands of convection surrounding an approximately symmetric eyewall and a central convection-free eye (details not shown).

(ii) Relative humidity

Following Bergeron (1950), recent work has hypothesized that a tropical depression vortex will begin to intensify only *after* the column-integrated relative humidity becomes nearly saturated on the *vortex scale* (Rotunno and Emanuel 1987; Emanuel 1989; Bister and Emanuel 1997; Raymond *et al.* 1998). The basis for this idea originates in observations showing that deep cumulus convection regions have adjacent downdrafts that advect middle tropospheric air possessing a minimum of moist entropy into the boundary layer (e.g., Zipser and Gautier 1978). Downdrafts originating near middle levels that manage to penetrate the boundary layer will dilute the high entropy content of the boundary layer, thereby rendering the lower troposphere less susceptible to deep convective activity and therefore to the buoyancy-induced convergence of angular momentum at low levels (M06).

To investigate the potential relationship between the intensification simulated in the control experiment and the middle tropospheric relative humidity (MRH) we have computed the average MRH from 700 hPa to 400 hPa over a circular region of 100 km in radius around the vortex centre. The time-series of this average MRH is shown in Fig. 2b. The average MRH increases from its initial value of 40% to 50% in the first hour and remains at this value for next 8 h. When rapid intensification begins at approximately 9 h, the average MRH increases from 50% to about 65% in about 7 h. This is because when a grid box in the lower troposphere is saturated, latent heat is released triggering deep convection. After 16 h, there is only a slight increasing trend from 65% to 75% at the end of the simulation. Therefore the moistening of the middle layer in the control experiment accompanies the rapid increase of the tangential wind field; it does not precede it.

As described in the previous section, the control experiment adopts the simplest explicit scheme available in MM5, i.e. as condensation occurs, the condensed water is immediately converted to precipitation and a commensurate amount of latent heat is released to the air; Evaporative cooling and related downdraft phenomenology is neglected (i.e., pseudo-adiabatic dynamics). A more sophisticated experiment that incorporates the warm rain process is discussed in section 5. Although downdrafts are found to temper the intensification rate and somewhat reduce the simulated maximum sustained winds, the basic picture presented using the simple scheme does not appear to be fundamentally different (not shown). The outcome of this experiment suggests that the control experiment captures the essence of the vortex intensification process.

(iii) Accumulated precipitation

It is of interest to determine the favoured regions of precipitation during the evolution. A high precipitation region is a good indication of active updrafts on the system scale. Twelve-hour accumulated precipitation at 12, 24, 48, and 96 h is shown in Fig. 3. Although one finds accumulated rainfall over the entire region shown, the regions of high accumulated rainfall are concentrated around the core of the developing vortex. With the exception of the first 12 h, the maximum twelve-hour accumulated rainfall reaches 400 mm at all times shown. In the outer region and within the eye, the accumulated rainfall is less than 80 mm. The qualitative characteristics of the highly precipitating regions are described below.

For the first 12 h, the accumulated precipitation is almost symmetric and distributed in two separate rings at approximately 70 and 100 km radius from the initial circulation centre. Early into the rapid intensification period (24 h) the accumulated precipitation exhibits some asymmetry manifest by localized anomalies within the precipitation annulus between 50 km and 70 km radius. Further into this period, at 48 h, the accumulated precipitation exhibits a pronounced asymmetry with the high rainfall found in the southeast sector of the vortex core. Between 84h and 96h, the precipitation field contracts and attains a distinct ring-like structure. The precipitation annulus now occupies the region between 30 km and 60 km. A careful examination of the pattern of the accumulated precipitation of ensemble members and their mean at 48 h shows that although there is a large difference between precipitation patterns among the ensemble members, the mean accumulated precipitation field is largely symmetric (not shown).

In order to obtain a deeper understanding of the physics of the intensification process in three dimensions, we turn now to examine the evolution of the vertical velocity and relative vorticity fields.

(iv) Vertical velocity structure

During the gestation period ($0 - 9$ h), there is only weak ascent at 850 hPa (above the boundary layer) in the vortex core region, within a radius of 150 km, and almost negligible ascent at 400 hPa (not shown). At 9 h, a narrow annulus of ascent is evident at 850 hPa, centred at 80 km radius, with a maximum value of approximately 0.7 m s^{-1} (not shown).

At the beginning of rapid intensification (9 h), latent heat release by saturation in some grid boxes initiates deep convective cells. From 9 h to 9.75 h, the annulus of ascent evolves into distinct localized updrafts with vertical velocity maxima between 2 and 5 m s^{-1}. These updrafts extend to much higher levels as shown in Fig. 4b, which illustrates their structure at 400 hPa. The distribution of the updrafts at 850 hPa shows a dominant azimuthal wavenumber-12 pattern around the circulation centre. During the same period (9 - 9.75 h), a second annulus of upward motion, centred at a radius of 110 km, forms outside the first annulus and vertical velocity maxima within it vary between 0.4 to 1 m s^{-1}. In the next 1.5 h (9.75 - 11.25 h), this outer ring of updrafts becomes dominant and the two updraft rings interact and transition into irregular cells (not shown). These cells rotate

DOI: 10.1002/qj

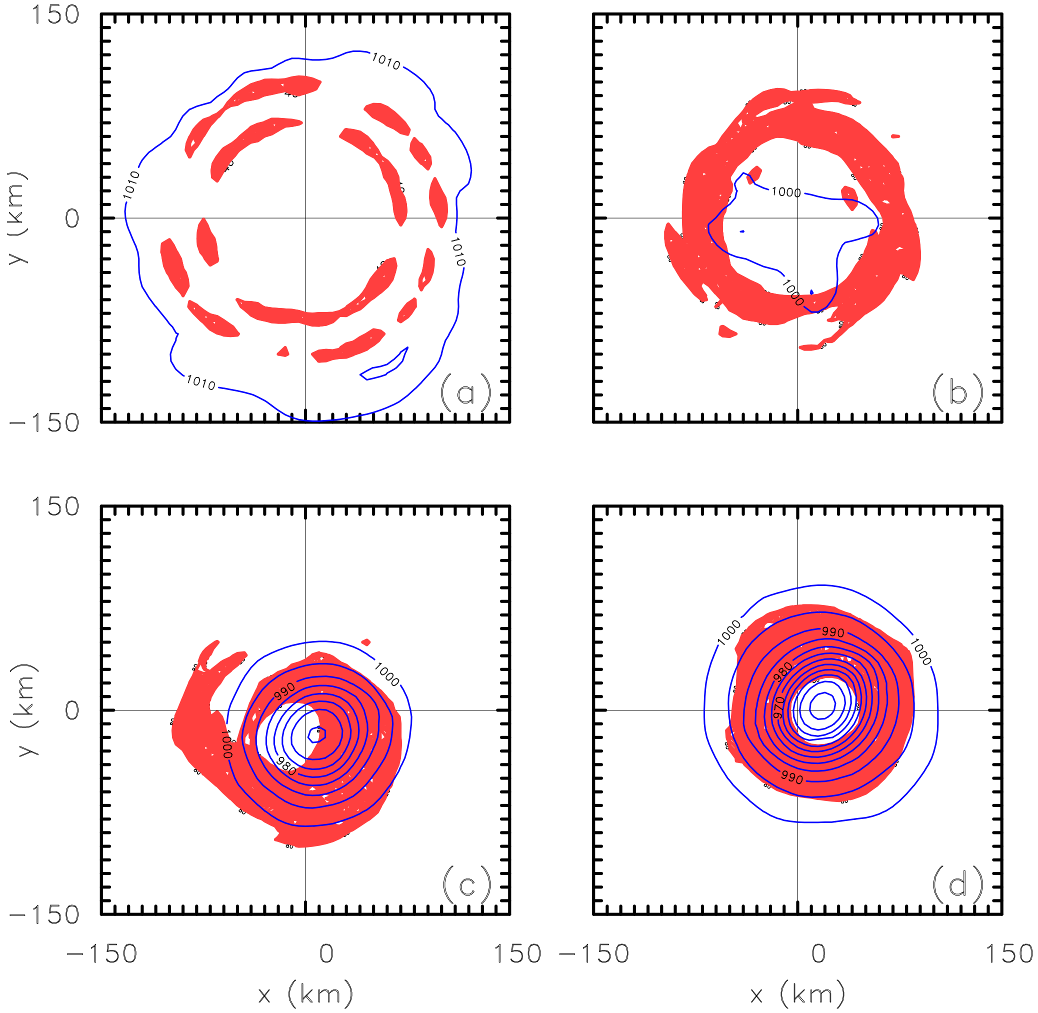

Figure 3. Surface pressure (contours, interval 5 hPa) and regions of 12 h accumulated precipitation exceeding 80 mm (40 mm in panel (a)) at (a) 12 h, (b) 24h, (c) 48h, (d) 96h for the control experiment C0. Maximum precipitation amounts are about 180 mm in (a), 400 mm in (b) and (c), and 450 mm in (d).

cyclonically around the vorticity centroid and are highly transient with a convective lifetime on the order of one hour. The updrafts at 400 hPa are nearly above the updraft cores at 850 hPa throughout the intensification process. The extrema of upward velocity in the updraft cores at 400 hPa are typically 2 to 3 times greater than at the corresponding 850 hPa level.

From 11.25 h to the end of the rapid intensification period (54 h), the updrafts increase in strength with local peak values attaining approximately 22 m s^{-1} at 400 hPa between 16 and 19 h (not shown). A snapshot of vertical motion at 24 h is shown in Fig. 4b. The structure of these updrafts are still spatially irregular. During some periods the upward motion occupies a contiguous region around the vortex centre (not shown). During rapid intensification the number of intense updrafts decreases from twelve at 9 h to no more than three by the end of the period of rapid intensification. The intense cells contract inward over time to a radius of approximately 35 km at 54 h. Evidence of spiral waves (gravity waves at the speed of approximately 40 m s^{-1}) propagating outwards is found throughout the vortex evolution (see, e.g. Fig. 4). From approximately 54 h onward, the structure of concentrated upward motion shows different patterns over time, but is mainly monopole, dipole, or tripole and always asymmetric.

(v) Relative vorticity structure

Snapshots of relative vorticity fields are shown in Figs. 5 and 6. The relative vorticity structure changes only slightly during the first 9 h, retaining its initial monopole structure. During this period the value of relative vorticity is approximately 4×10^{-4} s^{-1} at the centre of circulation. The updrafts that form at the beginning of the rapid intensification period (9 h) tilt and stretch the local vorticity field. An approximate ring-like structure of intense small-scale vorticity dipoles quickly emerges (Figs. 5b-d). This local dipolar structure in the relative vorticity occurs throughout the rapid intensification period. The vorticity dipoles are highly asymmetric with strong cyclonic vorticity anomalies and much weaker anticyclonic vorticity anomalies. Early in the intensification phase, the strong updrafts lie approximately in between the vorticity dipoles. Later in the intensification phase,

DOI: 10.1002/qj

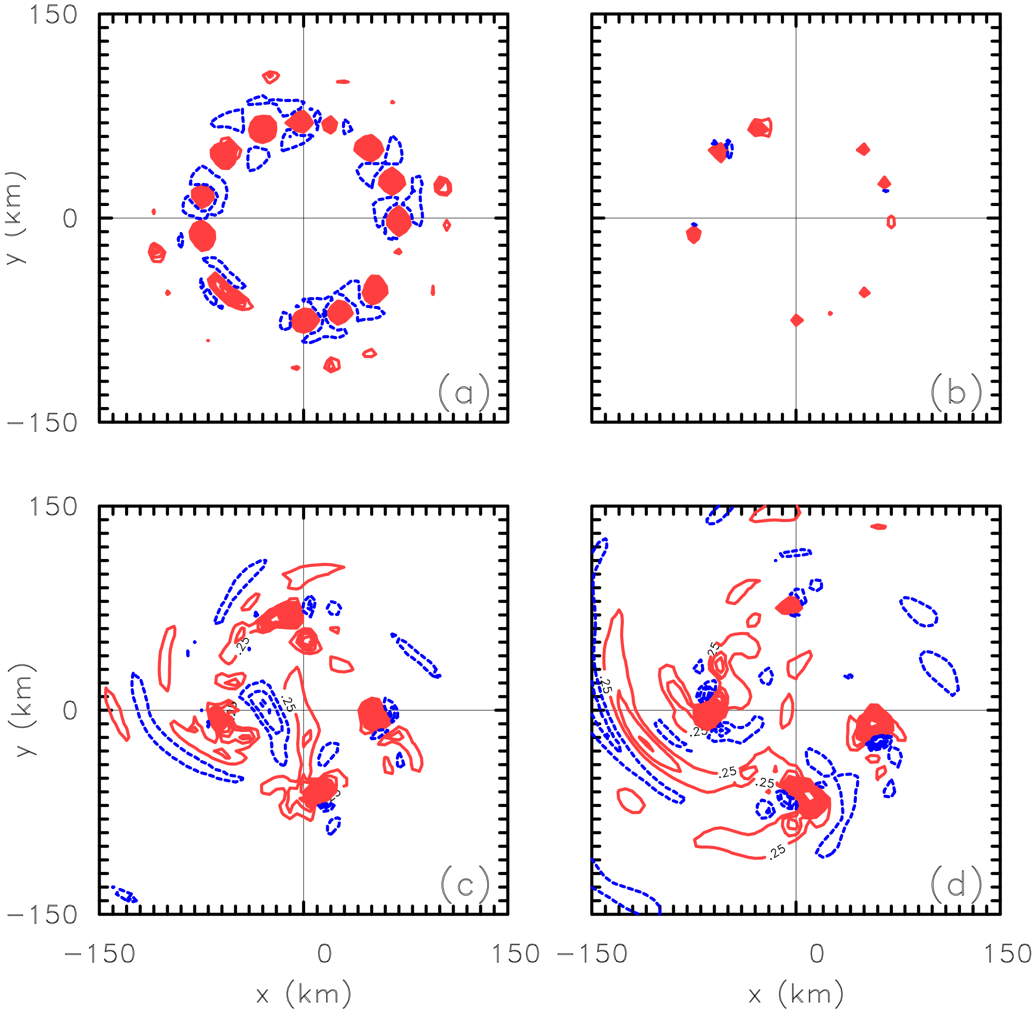

Figure 4. Vertical velocity fields at 850 hPa (left panels) and 400 hPa (right panels) at 9.75 h (panels a and b), 24 h (panels c and d) of the control experiment C0. Contour interval is 0.25 m s^{-1}. Negative values are in blue and dashed. The zero contour is not plotted.

strong updrafts are often approximately collocated with the strong cyclonic anomalies.

From approximately 12 h onwards, the VHTs are observed to grow horizontally in scale, in part due to merger and axisymmetrization with neighboring cyclonic vorticity anomalies and in part to convergence of like-sign vorticity from the nearby environment. During this time, the cyclonic anomalies move slowly inward, whereas the anticyclonic vorticity anomalies move slowly outward, decrease in amplitude and undergo axisymmetrization by the parent vortex. Because this vorticity segregation process occurs in the presence of persistent mean near-surface inflow and low- to upper-level outflow, the segregation process cannot be explained alone by the mean advection associated with the diabatically-forced axisymmeteric secondary circulation. Using prior work, a heuristic explanation of the segregation mechanism is offered here as a first step in a more detailed quantitative study.

Recall that vortex axisymmetrization involves the ingestion of like-sign vorticity anomalies accompanied by the formation of like-sign vorticity filaments surrounding the parent vortex as well as the expulsion of opposite-signed vorticity anomalies (Montgomery and Enagonio 1998). During the merger phase the amplitude of the cyclonic vorticity anomalies are approximately an order of magnitude larger than the background cyclonic vortex. Consequently the cyclonic anomalies are not easily axisymmetrized by the parent vortex. Since the initial vortex possesses a monotonic potential vorticity distribution a related vortex segregation mechanism is nonetheless available. From vortex motion theory (McWilliams and Flierl 1979, Smith and Ulrich 1990, Schecter and Dubin 1999), intense cyclonic vorticity anomalies generally "move up the ambient vorticity gradient" and vice versa for the anticyclonic vorticity anomalies. Therefore intense cyclonic anomalies immersed in the negative vorticity gradient of the parent vortex will tend to move toward the centre and the anticyclonic anomalies will tend to be move away; this segregation mechanism outweighs the low- to upper-level outflow and near-surface inflow, respectively. The divergent flow above the inflow layer weakens the anticyclonic anomalies leaving them susceptible to axisymmetrization. The end result is that during rapid intensification the VHTs make a direct contribution to the system-scale spin up (M06) and a mesoscale

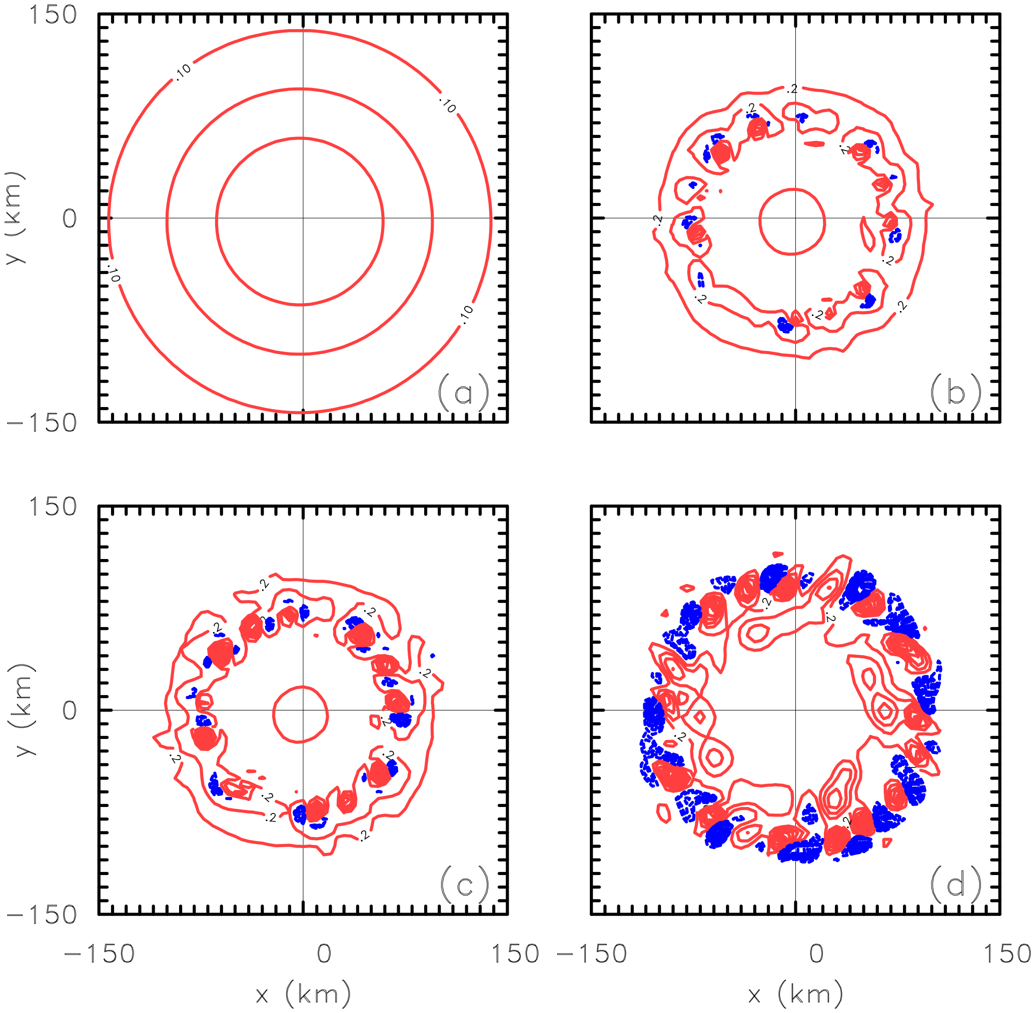

Figure 5. Vorticity fields at 850 hPa at (a) 0 h, (b) 9.75 h, (c) 10 h, (d) 12 h of the control experiment C0. Contour interval for positive values is 0.1×10^{-3} s^{-1} in panel a, 0.2×10^{-3} s^{-1} in panels b-d. Negative values are in blue and dashed with contour interval of 0.5×10^{-4} s^{-1}. The zero contour is not plotted.

inner-core region rich in cyclonic relative vorticity is constructed.

By the end of the rapid intensification period (approximately 54 h and onwards), no more than three VHTs are active around the circulation centre (not shown). The evolution of the vortex after the merging phase is presumably well described by vortex Rossby waves and their coupling to the boundary layer and convection (Montgomery and Kallenbach 1997, Chen and Yau 2003, Wang 2000a), but a more detailed analysis lies beyond the scope of this paper.

Based on the documented evolution of vertical velocity and relative vorticity fields, it is clear that the VHTs dominate the rapid intensification period at early times. A more in-depth and quantitative investigation of the dynamics of the VHTs and vortex Rossby waves and their contribution to the amplification of the system-scale vortex will be presented in due course.

3.2 Ensemble experiments on f-plane

In subsection (a), it was shown that the flow asymmetries that develop in the control experiment during the period of rapid intensification are associated with the development of model deep-convective VHTs. Although these VHTs form more or less within an annular envelope (Smith 1968; Eliassen and Lystad 1977), their precise location in the annulus is determined by local asymmetries associated with the representation of an initially symmetric flow on a square grid, which determine where grid-scale saturation first occurs. The symmetry would be expected to broken also if random perturbations of moisture were present in the boundary layer. In reality, it is well known that moisture is a quantity that has significant variability on small spatial scales (e.g. Weckwerth 2000). For this reason it is important to investigate the sensitivity of the inner-core asymmetries to perturbations in the low-level moisture distribution. To do this we have carried out an ensemble of experiments with an initially-perturbed moisture field at low levels (see Table I). The ensemble consists of ten members in which the moisture fields are initially perturbed at all levels below 950 hPa. A random perturbation in the range of (-0.5 g kg^{-1}, 0.5 g kg^{-1}) is added to the value of the moisture fields at every horizontal grid

DOI: 10.1002/qj

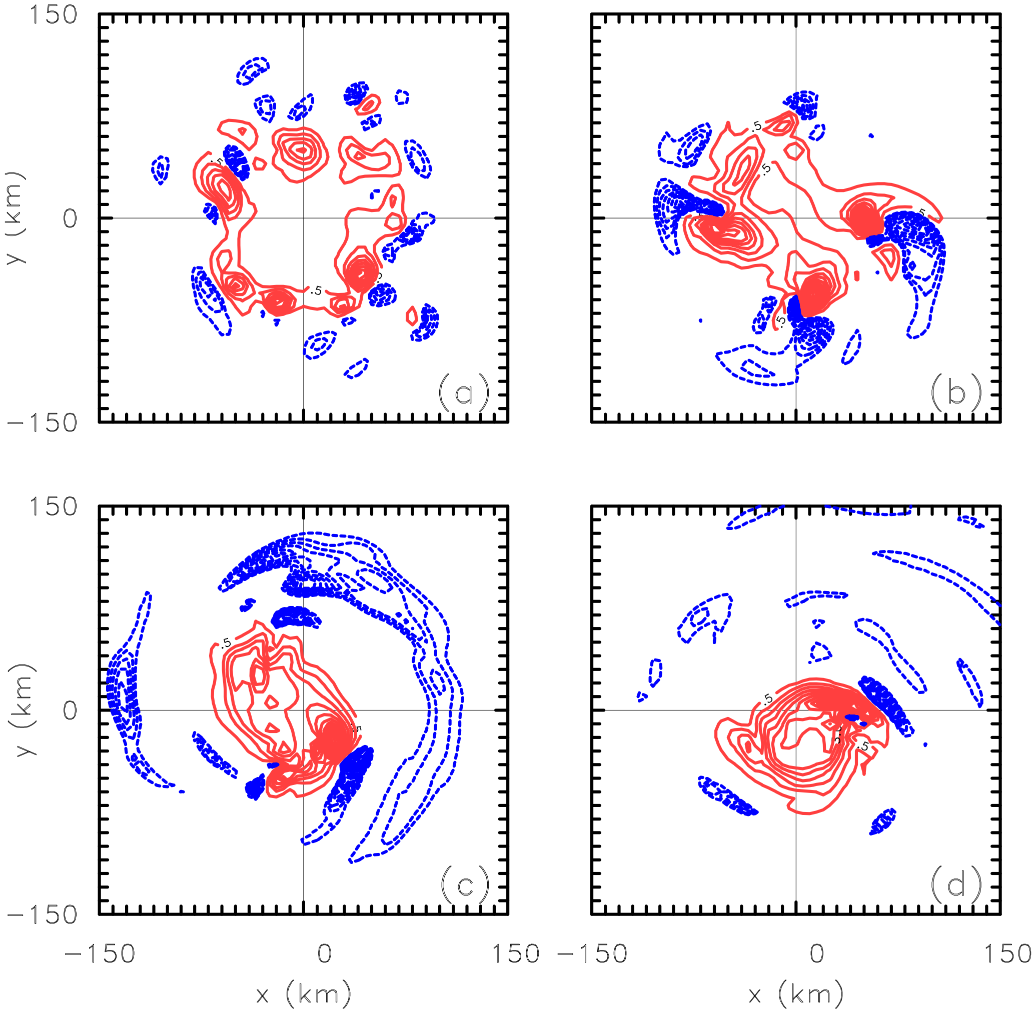

Figure 6. Vorticity fields at 850 hPa at (a) 18, (b) 24, (c) 36, (d) 48 h of the control experiment C0. Contour interval for positive values is 0.5×10^{-3} s^{-1}. Negative values are in blue and dashed with contour interval of 0.1×10^{-3} s^{-1} in panels a-b, 0.2×10^{-4} s^{-1} in panels c-d. The zero contour is not plotted.

point in the inner-most domain. This perturbation is different at each height. The temperature fields are recalculated from the original virtual temperature fields to keep the mass fields unchanged. All other aspects of the model configuration are unchanged.

(i) Intensity and inner-core structure

Figure 7a shows the time-series of the maximum of mean tangential wind speed of the control simulation and the ten member ensemble. Mean wind maxima of all ensemble members are close to each other until approximately 13 h. From that time onwards there is a spread in the simulated maxima. The spread occurs when the annular regions of high cyclonic relative vorticity of all members transition into irregular cells (not shown). The maximum difference between the mean intensity among all ensemble members at any given time in the whole simulation is approximately 12 m s^{-1}. All the ensemble simulations show the same rapid intensification period from 9 h to approximately 54 h and a slight increasing trend in intensity from approximately 54 h onward.

Figure 7b shows the time-series of maximum total wind speed VT_{max} for the same ensemble simulations. The spread in intensity occurs at approximately 10 h, sooner than the spread in mean tangential wind at approximately 14 h (Fig. 7a). The maximum difference between the VT_{max} among all ensemble members at any given time in the whole simulation is approximately 17 m s^{-1}. During the first hour of rapid intensification (9 to 10 h), there is a steep increase in intensity of all ensemble members. Since this time interval coincides with the appearance of the ring-like structure of small-scale vorticity dipoles, the VT_{max} is associated with the occurrence of VHTs. During the early time in the rapid intensification, the increase in VT_{max} occurs more rapidly and sooner than the increase of the maximum of mean tangential wind speed V_{max}. This feature reflects the fact that the flow intensifies first on the convective scales (VHTs), and subsequently the system-scale flow intensifies.

Figure 7 also shows that after the gestation period, especially during the rapid intensification phase, there is more variability between ensemble members in VT_{max} than in V_{max}. These results have important operational

DOI: 10.1002/qj

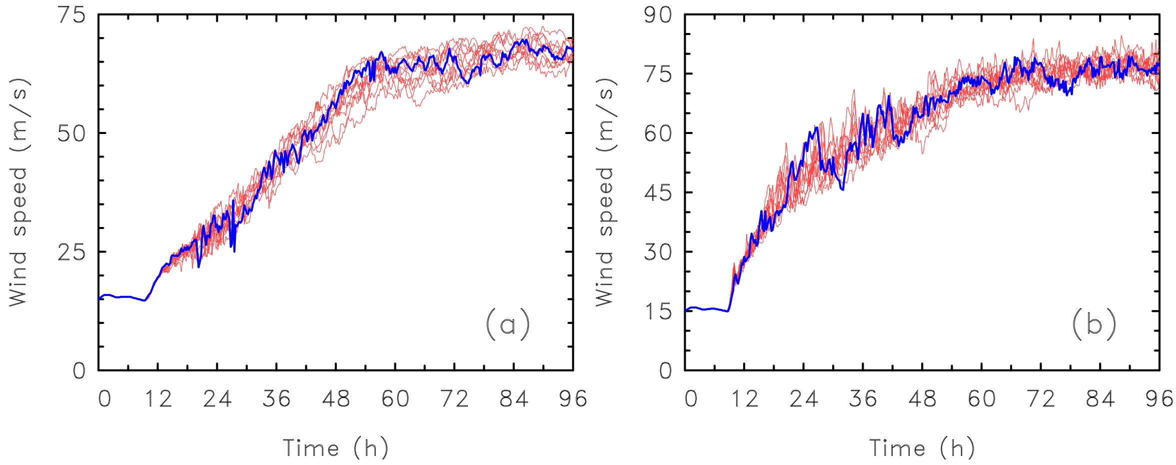

Figure 7. Time-series of (a) Azimuthal-mean maximum tangential wind speed, and (b) maximum total wind speed at 900 hPa in the control experiment C0 (blue) and in the 10 ensemble experiments (C1-C10).

implications in that the local wind speed can change quite dramatically during rapid intensification.

Inspection of relative vorticity fields of each ensemble member shows similar characteristics to those in the control experiment. The relative vorticity field is non-axisymmetric and the detailed pattern of small-scale vorticity structure is significantly changed. Figure 8 illustrates this point at a typical time during the rapid intensification process. We conclude that the ensuing evolution of VHTs exhibits a degree of randomness and is highly sensitive to the moisture distribution in the boundary layer. For all ensemble members, the vertical velocity is dominated by VHTs (see Fig.9).

(ii) Vortex-size parameters

We investigate now the development of two critical parameters on vortex size: the radius of maximum azimuthally-averaged tangential wind speed (RMW) and the radius of gale-force wind (RGW) (in general usage, gale-force wind refers to a sustained wind speed of 17 m s^{-1}). The former provides a scale for the region of extreme winds and for the eye size. The latter provides a scale for the region of potential significant damage.

Figure 10 shows time-series of the RMW and RGW in experiments C0-C10. During gestation period, the RMW expands from its initial value of 135 km to approximately 147 km, but after 5 h it starts to decrease rapidly. There is a spread in the RMW between ensemble members beginning with the rapid intensification period (9 to 54 h: see Fig. 2). There is a large variation of the RMW during this period, the difference between ensemble members being a maximum of approximately 32 km at 28 h. From 54 h onward, the RMW curves asymptote to a mean value of 35 km and the maximum difference among the ensemble members is approximately 7 km at 96 h.

The development of the radius of maximum total wind speed exhibits similar characteristics (not shown), but the variation among ensemble members is large during the rapid intensification period and also at later times. This is mainly because of the unpredictable and locally intense circulations associated with the VHTs (cf. Sec. 3a). The difference in the radius of maximum *total wind speed* among ensemble members reaches its maximum of approximately 70 km at 19 h and decreases to approximately 17 km at 96 h.

The maximum mean wind speed of all ensemble members exceeds gale-force at approximately 12 h. The RGW is calculated from that time onward by taking the outer radius at which the azimuthal-mean tangential wind speed equals 17 m s^{-1}. As shown in Fig. 10, the RGW quickly expands between 12 and 15 h. After that time, the RGW continues to grow for all ensemble members. From 24 h to 72 h, the variation is approximately 15 km. From 72 h onward, the variation is smaller (approximately 5 km) and there is an approximately linear increase with time for all ensemble members. All of the simulated hurricanes thus exhibit a real growth in horizontal size after the inner-core has reached a quasi-steady evolution.

Based on the results shown, it appears that the spread of the RMW and RGW decreases as the vortex approaches its quasi-steady maximum intensity. In contrast, the spread of maximum tangential wind speed and also total wind speed does not diminish as the quasi-steady state is reached. This result indicates that the RMW and RGW for the mature storm have less variability than, for example, V_{max}.

4 Experiments on a β-plane

In the previous section we showed that on an f-plane, the flow asymmetries that evolve are highly sensitive to the initial moisture distribution. Due in part to the practical connection of hurricane track to storm-scale asymmetries, it is of interest to enquire whether a similar result is true when there is a mechanism to force the asymmetries, such as occurs on a β-plane, or when a vortex is exposed to vertical wind shear in its environment. To investigate this question we have repeated all the above-mentioned experiments on a β-plane (see Table I). The effects of vertical wind shear will be investigated in a future paper.

DOI: 10.1002/qj

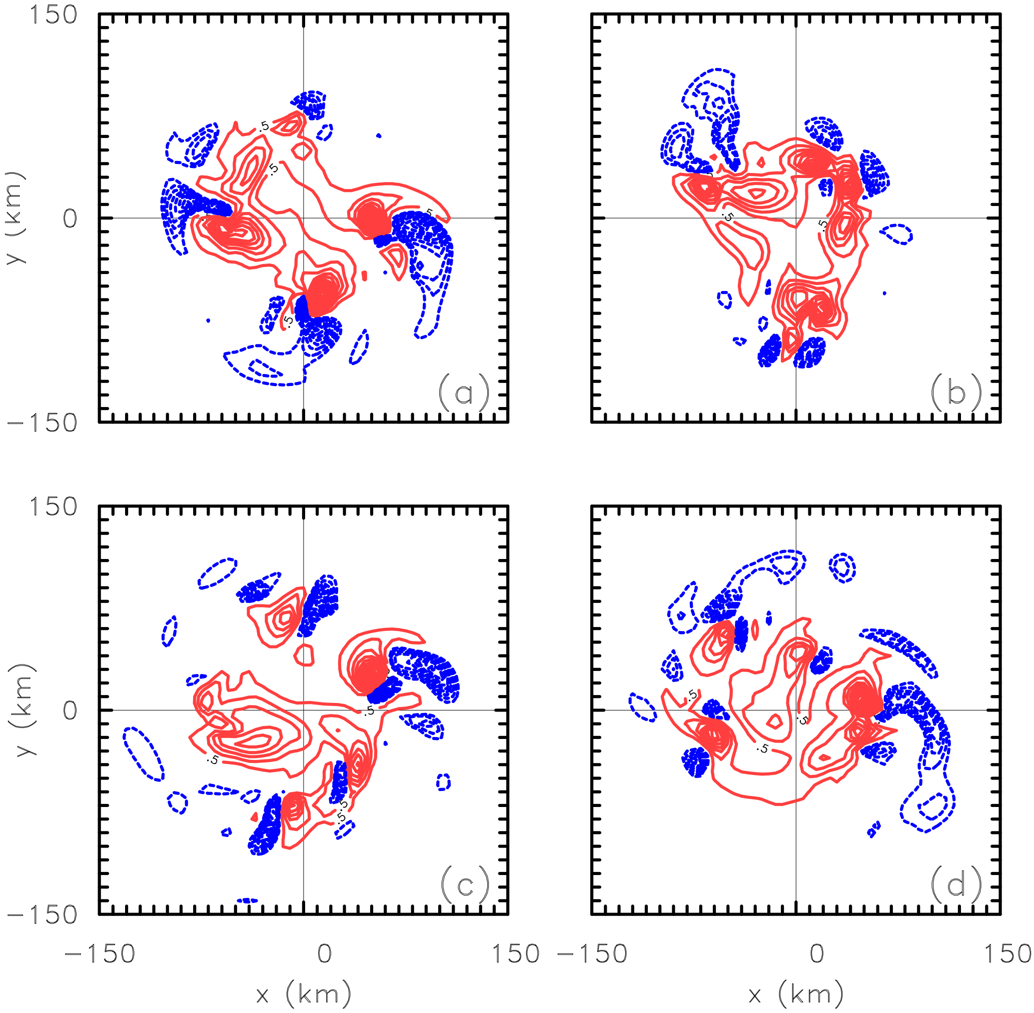

Figure 8. Relative vorticity fields of the control experiment C0 (panel a) and 3 representative realizations from the f-plane ensemble (panels b-d) at 24 h. Contour interval for positive value is 0.5×10^{-3} s^{-1}. Negative values are in blue and dashed with contour interval of 0.1×10^{-3} s^{-1}. The zero contour is not plotted.

Although the vortex moves north-northwest as a result of the β effect and the fields of accumulated precipitation are much more asymmetric than in the f-plane experiments (not shown), the main characteristics in the vortex core region are unchanged and the rapid intensification period is dominated by the VHTs.

It was shown in the previous section that there is about a 12 m s^{-1} spread in mean intensity of the ensemble members. The asymmetric forcing implied by the presence of β may be expected to produce an effect similar to a moisture perturbation on the initial pattern of convective cells. In order to determine whether there is a significant difference between the f- and β-plane experiments, one must compare the average of the ensemble means: it is insufficient just to compare two deterministic experiments. Figure 11a shows the ensenble average of the azimuthally-averaged tangential wind speed at 900 hPa as a function of time for the f-plane experiments C0-C10 and the β-plane experiments B0-B10. The curves lie close to each other with one higher for some periods and less for others. However, the difference between the two never exceeds 3 m s^{-1}. In particular, the differences lie well inside the intervals of the largest difference between any two members of either f-plane or β-plane ensemble experiments (indicated by the vertical bars). The spread found in the β-plane set is typically larger (no greater than 5 m s^{-1}) than that in the f-plane case. A similar diagram for minimum surface pressure is shown in Fig. 11b. It is clear that there is virtually no difference between the minimum surface pressure for f-plane and β-plane cases. On the basis of these results we conclude that the β-effect has essentially no impact on the maximum intensity of the vortex during the course of the simulations[‡].

In order to investigate the predictability of the vortex motion on the β-plane, the vortex centres of the experiments B0-B10 are calculated as discussed in Sec. 2. The results are shown in Fig. 12. The tracks start to spread after approximately 12 h and the maximum difference in relative position between any two members increases with

[‡]Our results differ profoundly from Kwok and Chan (2005), Wu and Braun (2004) and Peng *et al.* (1999) in regards to the influence of β on the simulated vortex intensity. These works found that β caused significant weakning, but they were limited by considerably coarser horizontal resolution and parameterized convection.

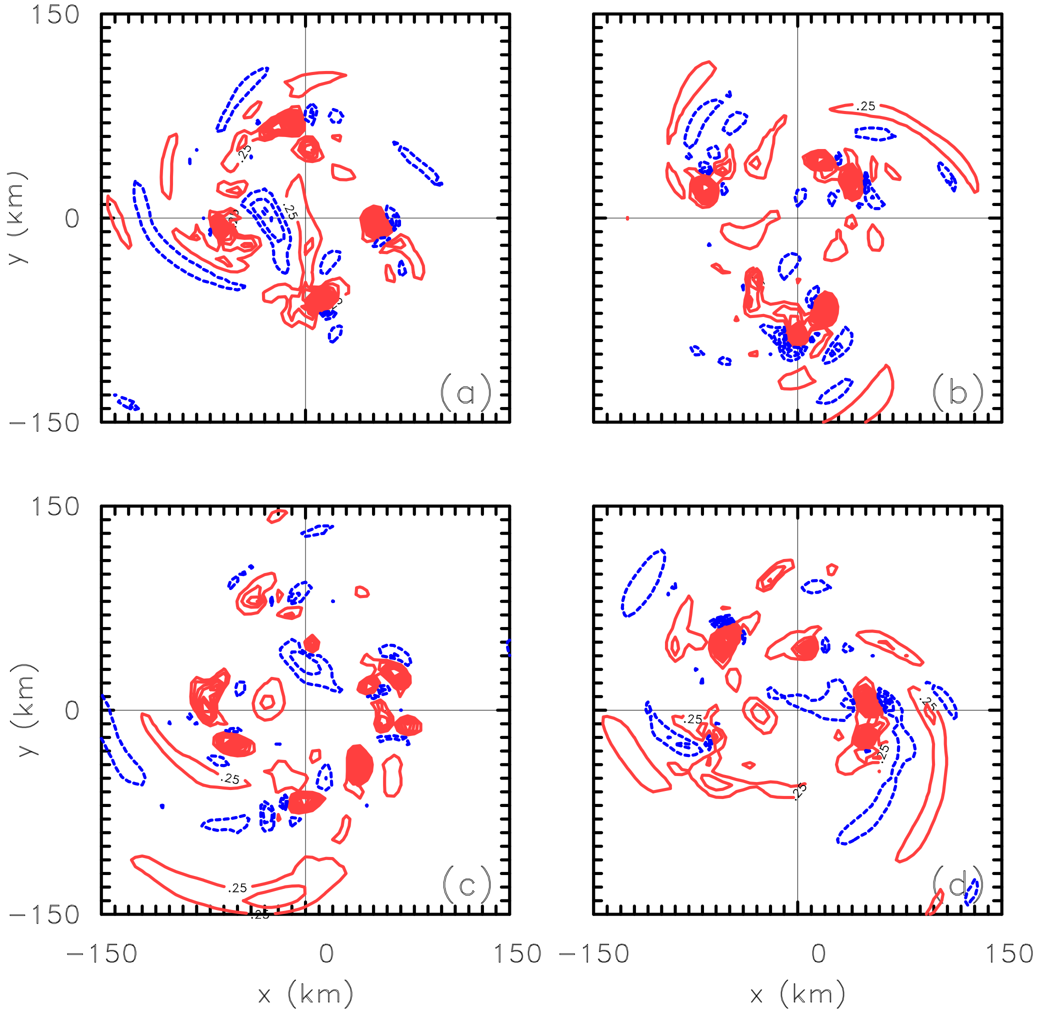

Figure 9. Vertical velocity fields of the control experiment C0 (top left) and 3 representative ensemble experiments at 24 h. Contour interval is 0.25 m s^{-1}. Negative values are in blue and dashed. The zero contour is not plotted.

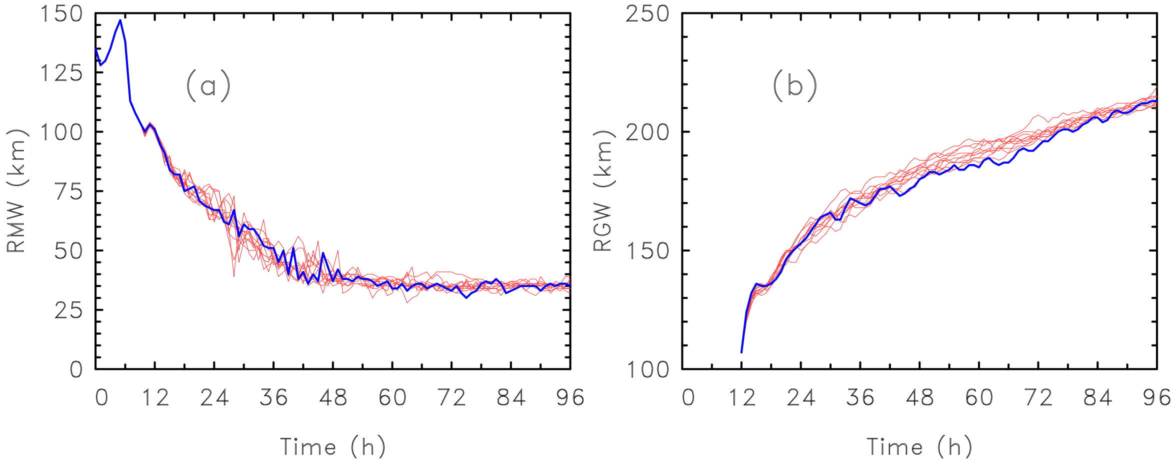

Figure 10. Time-series of radius of maximum mean tangential wind speed (a) and radius of gale force wind (b) of experiments C0 (blue) and C1-C10 (red).

time and is approximately 60 km at 96 h. The 60 km spread in the vortex tracks by day four provides a useful estimate of the track uncertainty associated with moisture perturbations in the boundary layer.

To confirm our expectation of the influence of the β-effect on the large-scale environment (e.g., Smith and Ulrich 1990; Smith and Weber 1993; Fiorino and Elsberry 1989), we consider the horizontal vorticity asymmetries of the ensemble experiments B0-B10 on all three domains. A combined multiple grid configuration of domains 1 (45

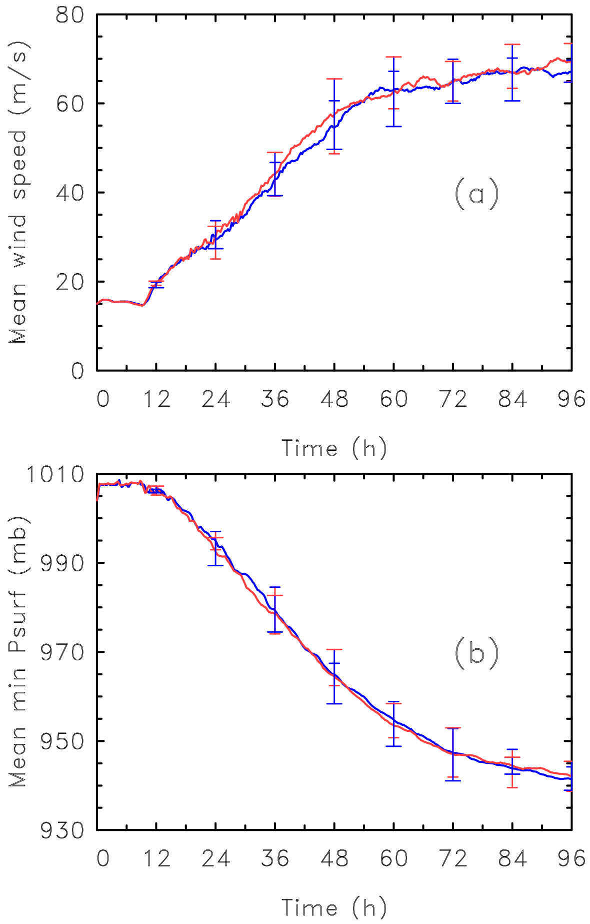

Figure 11. Ensemble average time series of: (a) the azimuthally-averaged tangential wind speed and (b) the minimum surface pressure of the f-plane experiments C0-C10 (blue line) and the β-plane experiments B0-B10 (red line). The corresponding vertical bars mark the maximum differences among ensemble members.

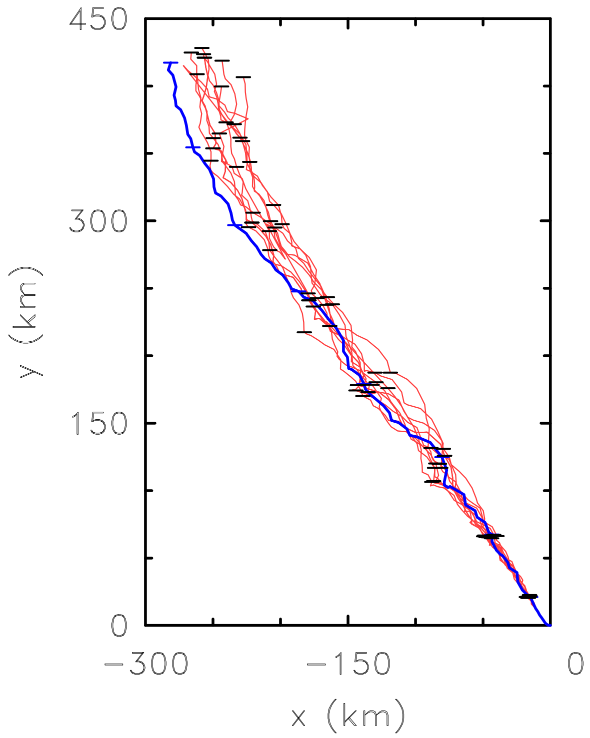

Figure 12. Tracks of vortex motion for β-plane experiments B0-B10. The tick marks on the tracks are every 12 h interval. The track of Expt. B0 is in blue.

km) and 2 (15 km) is set up as follows. First, domain 1 is interpolated to 15 km resolution and then domain 2 is projected onto the interpolated domain 1 where the data from domain 2 are defined. The vorticity asymmetry is calculated at each output time on the combined domain 1 and 2 by subtracting the axisymmetric relative vorticity from the total relative vorticity. Because the inner-most domain moves during the integration process, the inner-core asymmetries represented on domain 3 (5 km) are calculated separately and then projected onto the asymmetries of the combined domain 1 and 2 within 150 km from the vortex centre.

Figure 13 shows the ensemble-mean vorticity asymmetries of β-plane experiments B0-B10 on the 850 hPa surface at 48 h. In the inner-core region, the ensemble average asymmetry does not show a dominant wavenumber-one pattern. This has been verified at other times (not shown). For scales larger than the vortex's RMW, the pattern of the mean relative vorticity asymmetry has distinct β-gyres appearing at a radius of about 500 km from the vortex centre and the magnitude of these vorticity gyres is on the order of 10^{-5} s^{-1}. A β-gyre consists of a spiral band of cyclonic relative vorticity to the west of vortex centre and an anticyclonic relative vorticity band to the east. The standard deviation of ensemble members (not shown) is only appreciable within the radius of 200 km and is negligible outside this radius (less than 10 $^{-6}$ s^{-1}). Since the greatest difference between vorticity asymmetries among the ensemble members is confined to the inner-core region where the VHTs dominate, this implies that this difference of vorticity asymmetries between the ensemble members on the β-plane comes mainly from the VHTs. In other words, the large-scale β-gyres are virtually the same among all ensemble members.

Our conclusions in this section differ profoundly from those of a very recent paper by Ritchie and Frank (2007). They compared two deterministic experiments of a similar type to ours using also a similar version of MM5 with 5 km horizontal resolution. They found that the vortex on the β-plane "quickly develops a persistent wavenumber-one asymmetry in its inner core". Based on our ensemble experiments, we question the validity of this conclusion. Unfortunately, it is not possible to compare the details of vortex evolution in our control experiments with theirs as they show only coarse-grain, horizontal fields of potential vorticity and only at the mature stage of vortex development. Nevertheless, they did find little difference in the intensity between their f- and β-plane experiments, consistent with our findings.

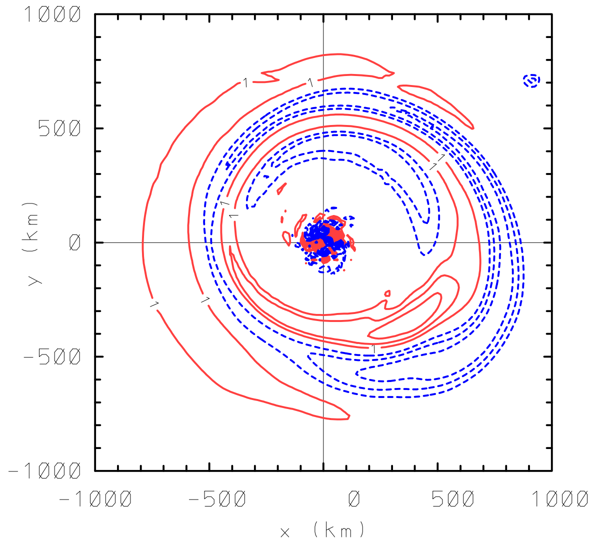

Figure 13. Ensemble mean relative vorticity asymmetry of β-plane experiments B0-B10 at 48 h at 850 hPa. Contour interval is 10^{-5} s^{-1}. Negative values are in blue and dashed. The zero contour is not plotted.

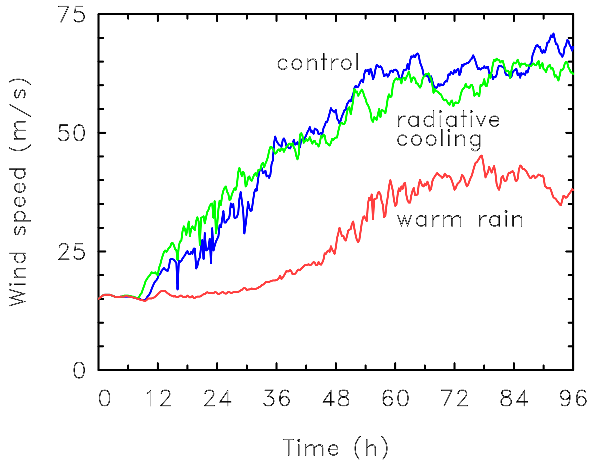

Figure 14. Time-series of azimuthal-mean maximum tangential wind speed at 900 hPa in the control experiment C0 and in the experiments with a representation of radiative cooling (S1) or warm rain processes (S2).

5 Sensitivity experiments

The control experiment described in section 3 is chosen to be as simple as possible, the main physics parameterizations being the bulk-aerodynamic boundary-layer scheme and a very simple explicit moisture scheme. Other potentially important processes such as evaporative downdrafts and radiative cooling are omitted. Here, we describe five additional experiments in which the sensitivity of vortex evolution to the inclusion of additional physical effects and to higher horizontal resolution is investigated. These experiments are detailed in Table II. The first, S1, explores the effects of radiative cooling using a simple scheme in which the temperature, T, in deg. Celsius is reduced everywhere by an amount $0.017T + 1.8$ per day[§].

The second experiment, S2, includes a warm-rain scheme, in which cloud and rain water are predicted explicitly in clouds. In this scheme, microphysical processes are represented by an empirical autoconversion function that converts cloud water to rain water. The rainwater falls with a terminal velocity that is a function of the mixing ratio for rainwater and it evaporates when the relative humidity falls below 100%. The cooling associated with the evaporation leads to resolved-scale downdrafts. Details of the scheme as coded in MM5 can be found in Grell *et al.* (1995) and Hsie and Anthes (1984). Two further experiments are designed to examine the role of surface fluxes. In experiment S3, no sensible and latent heat fluxes are allowed, while in experiment S4, there is an upper bound of 10 m s^{-1} on the wind speed in the formulae from which the sensible and latent heat fluxes are calculated. All these experiments have the same domain configuration as the control experiment C0. Finally, experiment S5 includes a fourth inner-most domain with a 1.67 km horizontal grid size. The results of these experiments are summarized below.

[§]In an experiment with no initial vortex this scheme produces scattered convection after approximately three days time. This radiation scheme is thus not ideal for long term simulations of a tropical cyclone, but should be adequate for assessing the basic influence of radiation on time scales of approximately three days or less.

With radiative cooling included (experiment S1), rapid intensification occurs about 2 h earlier than in the control experiment C0 (see Fig. 14). This is because with radiative cooling, the temperature of a grid column is slightly reduced so that grid-scale saturation occurs a little earlier. However, during the period of rapid intensification, the intensification rate is similar to that in the control experiment. In the mature stage the vortex intensity is higher than that of the control experiment for some periods and less for others. The developing vortex is found to be quanlitatively similar to that in the control experiment in that the asymmetries are still dominated by similar strength VHTs, but differ in detail in the same way that experiments C1 - C10 differ from C0 (see Figs. 15a and 15b). We conclude that radiative cooling has a minimal effect on the vortex evolution for the duration of the model integration.

When warm rain processes are included (experiment S2) (see Fig. 14), rapid intensification is delayed and the vortex intensifies more slowly than in the control experiment. On the time scale of four days the mature-stage intensity is lower also than that in C0, the peak maximum azimuthal-mean tangential wind being approximately 45 m s^{-1} at 77 h compared with 63 m s^{-1} at this time in C0. An extended experiment of S2 was carried out to determine the final maximum intensity at this resolution. At 384 h the maximum mean tangential wind is approximately 53 m s^{-1}. We attribute this behaviour to a reduction in the convective instability that results from convectively-driven downdrafts associated with the rain process and due to the reduced buoyancy in clouds on account of water loading. The VHTs emerge from approximately 10.5 h and are irregular and transient during the

DOI: 10.1002/qj

Table II. Sensitivity experiments.

No.	Name	Description
S1	Radiative cooling	Same as the control experiment (C0), but includes the simple cooling option for radiation scheme.
S2	Warm rain	Same as the control experiment, but includes the warm-rain scheme
S3	No heat flux	Same as the control experiment, but the surface latent and sensible heat fluxes are set to zero.
S4	Capped heat flux	Same as the control experiment, but the wind-speed dependence of the surface latent and sensible heat fluxes is suppressed beyond a wind speed of 10 m s^{-1}
S5	High horizontal resolution	Same as the control experiment, except that a fourth domain (300x300 km) is added with a horizontal grid size of 1.67 km.
S6	High vertical resolution	Same as the control experiment, except that the number of vertical levels was increased from 24 to 45.

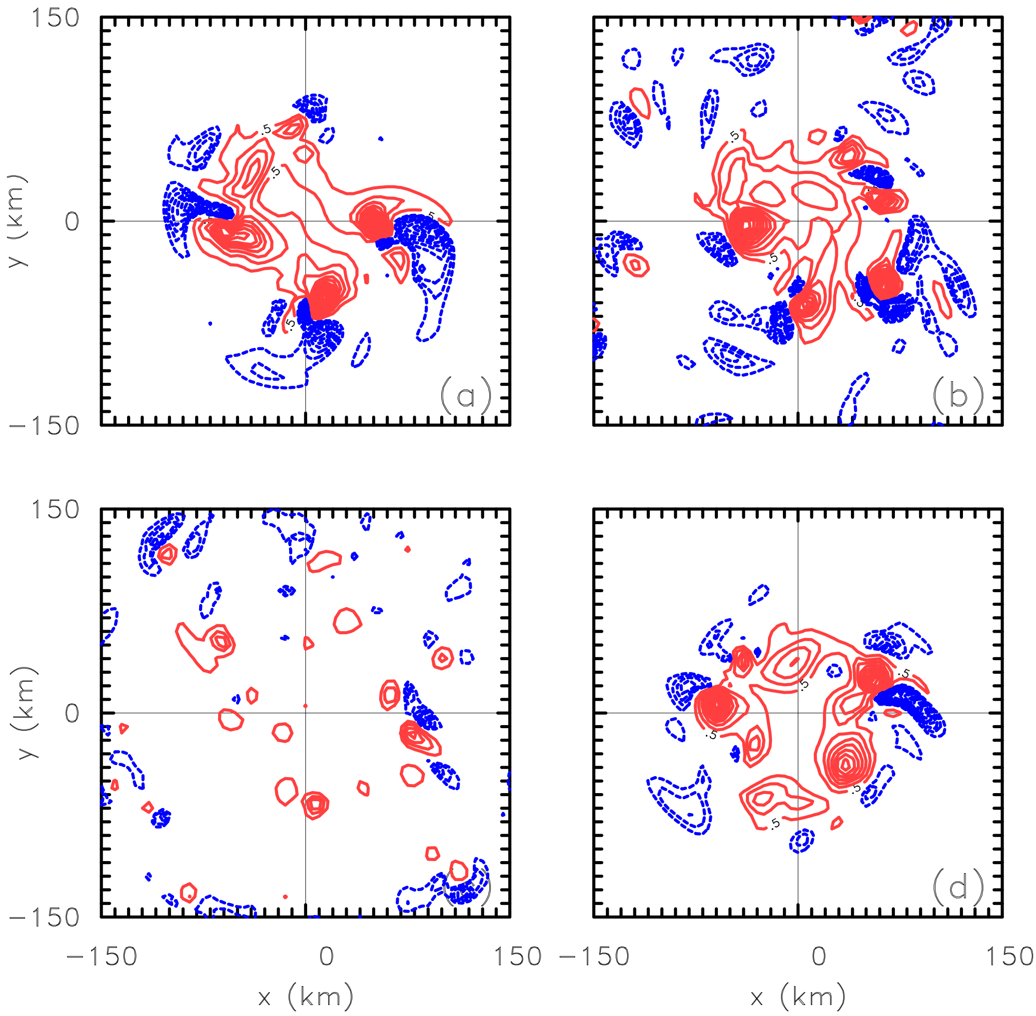

Figure 15. Vorticity fields at 850 hPa at 24 h of (a) Control experiment C0, (b) Radiative cooling S1, (c) Warm rain S2, (d) Capped heat flux S4. Contour interval for positive value is 0.5×10^{-3} s^{-1}. Negative values dashed with contour interval of 0.1×10^{-3} s^{-1}. The zero contour is not plotted.

period from 12 h to 36 h. The merging and axisymmetrization processes start later than in C0 from about 36 h to 60 h. The local extremes of relative vorticity are typically less than those in C0 (e.g., see Fig. 15c), although the qualitative characteristics of the intensification period are similar.

When the surface latent and sensible heat fluxes are suppressed entirely, (experiment S3), the vortex does not

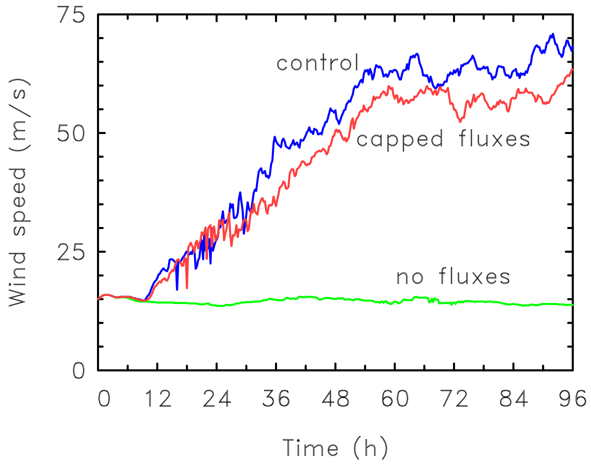

Figure 16. Time-series of azimuthal-mean maximum tangential wind speed at 900 hPa in the control experiment C0 and in the experiments with capped surface fluxes or no surface fluxes. In the experiments with capped surface fluxes, the wind speed dependence of both latent and sensible heat fluxes is suppressed beyond a wind speed of 10 m s^{-1}.

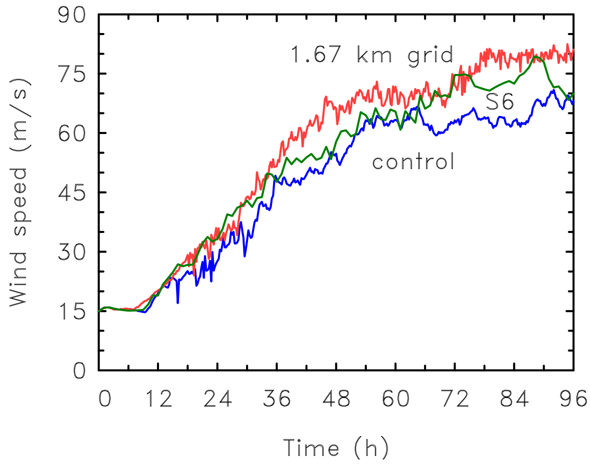

Figure 17. Time-series of azimuthal-mean maximum tangential wind speed at 900 hPa in the control experiment C0, in the experiment S5 with an increased horizontal grid resolution of 1.67 km in a fourth inner-most domain, and in the experiment S6 with an increased number of vertical levels to 45.

intensify (see Fig. 16), even though there is some transient hot-tower convection and local wind speed enhancement. The VHTs emerge at approximately 20 h, but then rapidly decrease in strength before they have the opportunity to merge (not shown). The local peak wind speed shows a slow decrease with time and this behavior is consistent with decaying VHTs that rapidly consume pre-existing Convective Available Potential Energy (CAPE) by convection, and receive no replenishment from latent heat fluxes in the boundary layer.

When the wind speed dependence of the surface latent and sensible heat fluxes is capped at a wind speed of 10 m s^{-1} (experiment S4), the evolution of maximum mean tangential wind is similar to that in the control experiment until 30 h (see Fig. 16). After this time, it is generally less than that of the control experiment, but the difference between the two at any time never exceeds 10 m s^{-1}. The intensification process is still dominated by VHTs. The maximum VHT strength has approximately the same amplitude to that in the control experiment during intensification process (see Fig. 15d). On the system-scale, late into the intensification period and in the mature state, the vorticity anomalies are slightly weaker than in the control experiment. Based on this evidence we conclude that the intensification occurs not as a result of pre-existing CAPE, but rather the modest replenishment of boundary layer θ_e by sea-to-air latent heat fluxes. *This is an important finding because it demonstrates that a positive feedback between water vapour flux and cyclone wind speed is not essential for tropical-cyclone intensification and maintenance as proposed by Rotunno and Emanuel (1987) in their axisymmetric experiments.* This result has been found to be robust to the inclusion of cloud water and evaporatively cooled downdrafts (not shown). It has been confirmed also in a high spatial and temporal resolution re-run of the Rotunno and Emanuel (1987) experiment J with speed-capped sea-to-air fluxes of latent and sensible heat (capping also the coefficients of exchange of latent and sensible heat) (J. Persing, personal communication). These and other aspects of the capped-wind-speed flux experiments as well as a more in-depth examination of the differences between the three-dimensional and axisymmetric intensification mechanisms will be reported in forthcoming work.

In the high-horizontal-resolution experiment (S5), the smaller grid size enables grid-scale saturation to occur sooner, which is reflected in the fact that rapid intensification begins at about 6 h, 3 h earlier than in the control experiment (Fig. 17). The mature-stage intensity is higher than in the control with V_{max} approximately 70 m s^{-1} at 54 h and 80 m s^{-1} at 96 h. The RMW during the mature state is approximately 30 km, slightly less than that of the control experiment (approximately 35 km). The maximum *local* wind speed VT_{max} approaches 90 m s^{-1} at 96 h. From these results there is clear evidence of an increase in intensity with increased horizontal resolution. The tendency of the simulated intensity to increase substantially at higher resolution has been documented in the literature (Persing and Montgomery 2003, Hausman *et al.* 2006), but a detailed examination of this issue in three dimensions is beyond the scope of current work¶.

At the beginning of rapid intensification in experiment S5 (Fig. 18a), many more VHTs form in an annular region than in the control experiment. Nevertheless the behaviour of VHTs during the intensification phase is similar to that in C0, the ensemble experiments and physics sensitivity experiments, with cyclonic vorticity skewness

¶This simulated hurricane and that of the control experiment have been verified to be "superintense" as defined by Persing and Montgomery (2003). These numerical experiments support the hypothesis that the superintensity phenomenon persists in three-dimensions (Montgomery *et al.* 2006b).

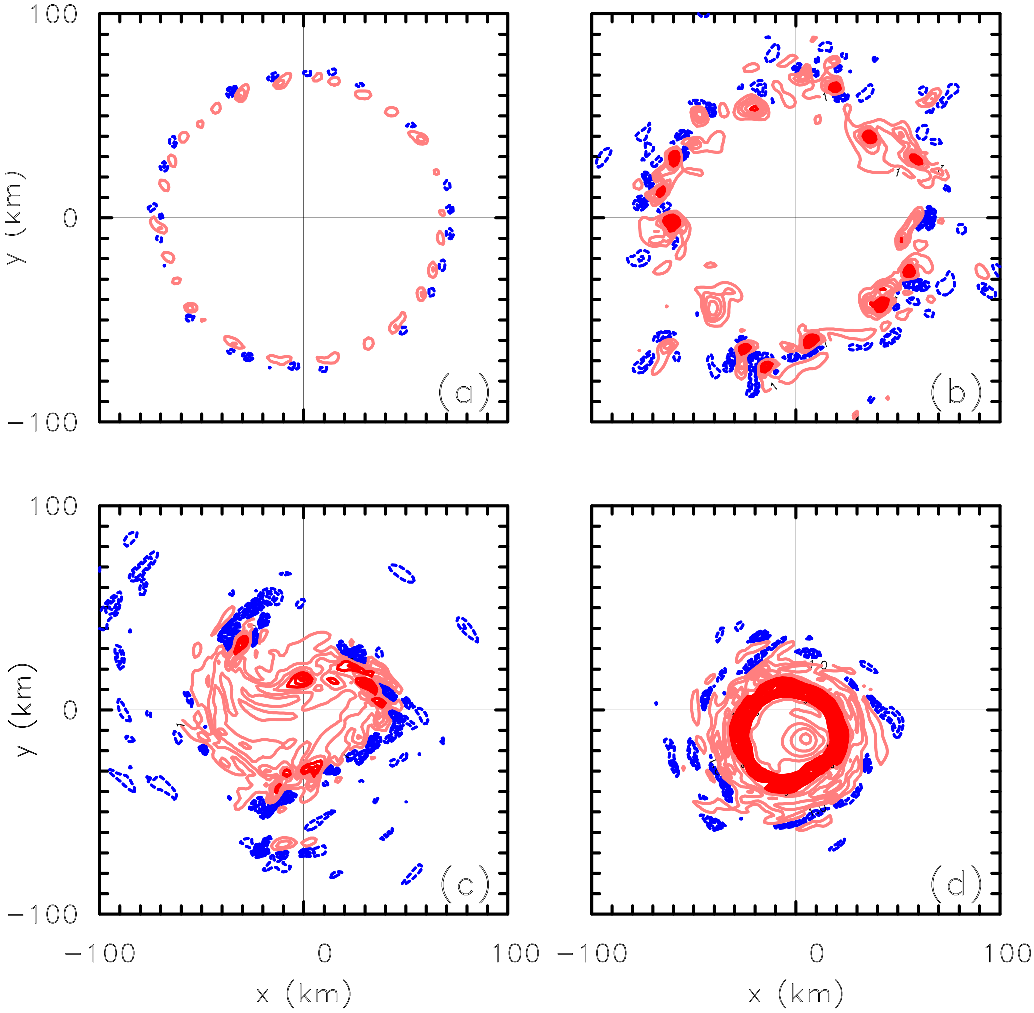

Figure 18. Vorticity fields at 850 hPa at (a) 7 h, (b) 18 h, (c) 36 h, (d) 78 h of 1.67 km experiment (S5). Contour interval for positive values is 10^{-3} s^{-1}. The zero contour is not plotted. Regions with value exceeding 5×10^{-3} s^{-1} are in dark red. Negative values dashed with contour interval of 0.5×10^{-3} s^{-1} in panels a-b, 0.2×10^{-3} s^{-1} in panels c-d.

in the lower troposphere, segregation of cyclonic and anticyclonic vorticity anomalies, axisymmetrization of anticylonic vorticity anomalies, and ultimately the establishment of a mesoscale inner-core region rich in cyclonic vorticity (e.g., Fig. 18c). After the VHT segregation and merger phase subsides (from approximately 50 h onward), a distinct eyewall forms with an approximate ring of enhanced cyclonic vorticity (Fig. 18d) (In this sense the control results at 5 km horizontal grid spacing are not yet converged). This eyewall structure persists beyond this time. Vorticity patterns in the eyewall region take multiple forms, ranging from pentagons, squares, triangles, ellipses and circles. Complete breakdown of the eyewall is not observed, however (cf. Schubert *et al.* 1999). The evolution is consistent with the picture of propagating near-discrete and sheared vortex Rossby waves and localized mixing events between the eyewall and its interior/exterior.

One candidate explanation for the persistence of an elevated vorticity ring is that the sustained convergence of the secondary circulation acts to temper the shear instability that has been demonstrated previously in unforced hurricane-like vortices (Montgomery *et al.* 2002, Nolan 2001; cf. Kossin and Schubert 2001 and Schubert *et al.* 1999). In a complimentary study the cloudiness that pervades hurricane eyewalls has been suggested also to temper these shear instabilities (Schecter and Montgomery 2007). These explanations are not mutually exclusive and a more in-depth study of this topic will be presented in due course.

We have carried out also a high-vertical-resolution experiment (S6) in which the horizontal resolution is unchanged from experiment C0 but the number of vertical levels was increased from 24 to 45. The additional vertical levels are added so that $\delta\sigma$ is half that of the control experiment in every vertical interval except th lowest two (because the vertical resolution there is already sufficient). Figure 17 shows that the mean vortex in experiment S6 is generally more intense than in the control C0. We believe that the reason for this is due to the increased resolution of the region where the inflow turns upwards and flows radially outwards to the eyewall, which more accurately represents the moist entropy flux from the low-level eye into the eyewall. This low-level eye air possesses

DOI: 10.1002/qj

higher equivalent potential temperature than air found at the RMW due to a lower surface pressure and nonzero surface winds and contributes additional heat and local buoyancy to the eyewall. The net result is an enhancement of the radial gradient of equivalent potential temperature above the inflow layer that supports strong tangential winds in accordance with axisymmetric thermal wind balance above the boundary layer (Montgomery *et al.* 2006b, Appendix). We have verified that the evolution in S6 is similar to that presented for experiment C0. These findings confirm the dominance and intrinsic randomness of the VHTs during the intensification phase‖.

In summary, the vortex evolution during the merger phase in all the sensitivity experiments is dominated by VHT activity, except in the no flux experiment S3, and the intensification process is similar to that in the control experiment.

6 Conclusions

On the evidence presented above we conclude that the inner-core flow asymmetries in a tropical cyclone are random intrinsically unpredictable. This lack of predictability is a reflection of the convective nature of the inner-core region and extends to the prediction of intensity itself. Deep convective towers growing in the rotation-rich environment of the incipient core amplify the local vertical rotation. These so-called “vortical hot towers” (VHTs) are the basic coherent structures of the intensification process, which itself is intrinsically asymmetric and random in nature. In the numerical experiments presented herein it is the progressive segregation, merger and axisymmetrization of these towers and the low-level convergence they generate that is fundamental to the intensification process, but axisymmetrization is never complete. There is always a prominent low azimuthal wavenumber asymmetry (often wavenumber one or two) of the inner-core relative vorticity.

The wind-induced surface heat exchange (WISHE) feedback mechanism that has been proposed previously to explain tropical-cyclone intensification in an axisymmetric framework has been found to be much less of a constraint in three dimensions because the VHTs are able to extract locally sufficient surface moisture fluxes necessary for their growth without the wind-moisture feedback that typifies WISHE. The tendency of the simulated hurricane intensity to surpass its predicted upper bound at high resolution has been verified here using the simplest explicit latent heating scheme with instantaneous rain fallout (pseudo-adiabatic dynamics).

Finally, even though the effect of β imposes a wavenumber-one forcing of the flow asymmetries and concomitant northwestward vortex motion, the inner-core behaviour is essentially the same as that on the f-plane and again dominated by VHTs and vortex Rossby waves..

‖Kimball and Dougherty (2006) examined the sensitivity of idealized hurricane structure and development to the distribution of vertical model levels and found that vortex intensity is also sensitive to this distribution. Our calculations here show that the basic intensification process is independent of the vertical resolution.

7 Acknowledgements

This research was supported in part by Grant No. N00014-03-1-0185 from the U.S. Office of Naval Research and by National Science Foundation Grants ATM-0715426, ATM-0649943, ATM-0649944, and ATM-0649946. The first author is grateful for tralvel support provided by the German Research Council (DFG) as part of the Project ”Improved quantitative precipitation forecasting in Vietnam.”

References

Bergeron, T., 1950: Über der mechanismus der ausgiebigan niederschläge. *Ber. Dtsch. Wetterd.*, **12**, 225-232.

Bister, M. and K. Emanuel, 1997: The genesis of Hurricane Guillermo: TEXMEX analyses and a modeling study. *Mon. Wea. Rev.*, **125**, 2662-2682.

Black, M. L., J. F. Gamache, F. D. Marks Jr., C. E. Samsury, and H. E. Willoughby, 2002: Eastern Pacific Hurricanes Jimena of 1991 and Olivia of 1994: The effect of vertical shear on structure and intensity. *Mon. Wea. Rev.*, **130**, 2291-2312.

Blackwell, K. G., 2000: The Evolution of Hurricane Danny (1997) at Landfall: Doppler-Observed Eyewall Replacement, Vortex Contraction/Intensification, and Low-Level Wind Maxima. *Mon. Wea. Rev.*, **128**, 4002-4016.

Braun, S. A., 2002: A cloud-resolving simulation of Hurricane Bob (1991): Storm structure and eyewall buoyancy. *Mon. Wea. Rev.*, **130**, 1573-1592.

Braun, S. A., M. T. Montgomery, and Z. Puc, 2006: High-Resolution Simulation of Hurricane Bonnie (1998). Part I: The Organization of Eyewall Vertical Motion. *J. Atmos. Sci.*, **63**, 19-42.

Chen, Y., and M. K. Yau, 2001: Spiral bands in a simulated hurricane. Part I: vortex Rossby wave verification. *J. Atmos. Sci.*, **58**, 2128-2145.

Chen, Y., G. Brunet, and M. K. Yau, 2003: Spiral Bands in a Simulated Hurricane. Part II: Wave Activity Diagnostics. *J. Atmos. Sci.*, **60**, 1239-1256.

Davis, C. A., and L. F. Bosart, 2002: Numerical simulations of the genesis of Hurricane Diana (1984). Part II: Sensitivity of track and intensity prediction. *Mon. Wea. Rev.*, **130**, 1100-1124.

Dengler, K., and M. J. Reeder, 1997: The effects of convection and baroclinicity on the motion of tropical-cyclone-like vortices. *Quart. J. Roy. Meteor. Soc.*, **123**, 699-727.

Dudhia, J., 1993: A non-hydrostatic version of the Penn State-NCAR mesoscale model: Validation tests and simulation of an Atlantic cyclone and cold front. *Mon. Wea. Rev.*, **121**, 1493-1513.

Eliassen, A., and M. Lystad, 1977: The Ekman layer of a circular vortex: A numerical and theoretical study. *Geophys. Norv.*, **31**, 1-16.

Emanuel, K. A., 1989: The finite amplitude nature of tropical cyclogenesis. *J. Atmos. Sci.*, **46**, 3431-3456.

Emanuel, K. A., 1995: Sensitivity of tropical cyclones to surface exchange coefficients and a revised steady-state model incorporating eye dynamics. *J. Atmos. Sci.*, **52**, 3969-3976.

Enagonio, J., and M. T. Montgomery, 2001: Tropical cyclogenesis via convectively forced vortex Rossby waves in a shallow water primitive equation model. *J. Atmos. Sci.*, **57**, 685-706.

Fiorino, M., and R. L. Elsberry, 1989: Some aspects of vortex structure related to tropical cyclone motion. *J. Atmos. Sci.*, **46**, 975-990.

Flatau, M., W. H. Schubert, and D. E. Stevens, 1994: The role of baroclinic processes in tropical cyclone motion: The influence of vertical tilt. *J. Atmos. Sci.*, **51**, 2589-2601.

Frank, W. M., and E. A. Ritchie, 1999: Effects of environmental flow upon tropical cyclone structure. *Mon. Wea. Rev.*, **127**, 2044-2061.

Frank, W. M., and E. A. Ritchie, 2001: Effects of vertical wind shear on hurricane intensity and structure. *Mon. Wea. Rev.*, **129**, 2249-2269.

Grell, G. A., J. Dudhia, and D. R. Stauffer, 1995: A description of the fifth generation Penn State/NCAR mesoscale model (MM5). NCAR Tech Note NCAR/TN-398+STR, 138 pp.

Hausman S. A. , K. V. Ooyama, and W. H. Schubert, 2006: Potential Vorticity Structure of Simulated Hurricanes. *J. Atmos. Sci.*, **63**, 87-108.

Hendricks, E. A., M. T. Montgomery, and C. A. Davis, 2004: On the role of “vortical” hot towers in formation of tropical cyclone Diana (1984). *J. Atmos. Sci.*, **61**, 1209-1232.

Heymsfield, G. M., J. B. Halverson, J. Simpson, L. Tian, and T. Paul Bui, 2001: ER-2 Doppler Radar Investigations of the Eyewall of Hurricane Bonnie during the Convection and Moisture Experiment-3. *J. Appl. Meteor.*, **40**, 1310-1330.

Hsie, E.-Y. and R. A. Anthes, 1984: Simulations of frontogenesis in a moist atmosphere using alternative parameterizaton of condensation and precipitation. *J. Atmos. Sci.*, **41**, 2701-2716.

Jones, S. C., 1995: The evolution of vortices in vertical shear. Part I: Initially barotropic vortices. *Quart. J. Roy. Meteor. Soc.*, **121**, 821-851.

Kimball, S. K. and F. C. Dougherty, 2006: The Sensitivity of Idealized Hurricane Structure and Development to the Distribution of Vertical Levels in MM5. *Mon. Wea. Rev.*, **134**, 1987-2008.

Kossin, J. P., and W. H. Schubert, 2001: Mesovortices, polygonal flow patterns, and rapid pressure falls in hurricane-like vortices. *J. Atmos. Sci.*, **58**, 2196 - 2209.

Kurihara, Y., M. Bender, R. Tuleya, and R. Ross, 1990: Prediction experiments of Hurricane Gloria (1985) using a multiply nested movable mesh model. *Mon. Wea. Rev.*, **118**, 2185-2198.

Kwok, H. Y. and J. C. L. Chan, 2005: The influence of uniform flow on tropical cyclone intensity change. *J. Atmos. Sci.*, **62**, 3193-3212.

Lorenz, E. N., 1969: The predictability of a flow which possesses many scales of motion. *Tellus*, **21**, 289-307.

Marks F. D. Jr., and R. A. Houze Jr., 1984: Airborne Doppler Radar Observations in Hurricane Debby. *Bull. Amet. Soc. Meteor.*, **65**, 569-582.

McWilliams, J. C., and G. R. Flierl, 1979: On the evolution of isolated nonlinear vortices. *J. Phys. Oceanogr.*, **9**, 1155 - 1182.

Möller, J. D., and M. T. Montgomery, 1999: Vortex Rossby Waves and Hurricane Intensification in a Barotropic Model. *J. Atmos. Sci.*, **56**, 1674-1687.

Möller, J. D., and M. T. Montgomery, 2000: Tropical cyclone evolution via potential vorticity anomalies in a three-dimensional balance model. *J. Atmos. Sci.*, **57**, 3366-3387.

Montgomery, M. T., and R. J. Kallenbach, 1997: A theory for vortex Rossby waves and its application to spiral bands and intensity changes in hurricanes. *Quart. J. Roy. Meteorol. Soc.*, **123**, 435 - 465.

Montgomery, M. T., and J. Enagonio, 1998: Tropical cyclogenesis via convectively forced vortex Rossby waves in a three-dimensional quasi-geostrophic model. *J. Atmos. Sci.*, **55**, 3176-3207.

Montgomery, M. T., V. A. Vladimirov, and P. V. Denissenko, 2002: An experimental study on hurricane mesovortices. *J. Fluid. Mech.,* **471**, 1-32.

Montgomery, M. T., M. E. Nicholls, T. A. Cram, and A. B. Saunders, 2006a: A vortical hot tower route to tropical cyclogenesis. *J. Atmos. Sci.*, **63**, 355-386.

Montgomery, M. T., M. M. Bell, S. D. Aberson, and M. L. Black, 2006b: Hurricane Isabel (2003): New insights into the physics of intense storms. Part I Mean vortex structure and maximum intensity estimates. *Bull. Amer. Meteorol. Soc.*, **87**, 1335 - 1348.

Musgrave, K. D., C. A. Davis, M. T. Montgomery, 2006: Hurricane Gabrielle (2001), submitted to *J. Atmos. Sci.*

Nguyen, C. M., R. K. Smith, H. Zhu, and W. Ulrich, 2002: A minimal axisymmetric hurricane model. *Quart. J. Roy. Meteor. Soc.*, **128**, 2641-2661.

Nolan, D. S., 2001: The stabilizing effects of axial stretching on turbulent vortex dynamics. *Phys. Fluids*, **13**, 1724-1738.

Ooyama, K. V., 1969: Numerical simulation of the life cycle of tropical cyclones. *J. Atmos. Sci.*, 26, 3-40.

Peng, M. S., B.-F. Jeng, and R. T. Williams, 1999: A numerical study on tropical cyclone intensification. Part I: Beta effect and mean flow effect. *J. Atmos. Sci.*, **56**, 1404-1423.

Persing, J., and M. T. Montgomery, 2003: Hurricane Superintensity. *J. Atmos. Sci.*, **60**, 2349-2371.

Raymond, D. J., H. Jiang, 1990: A theory for long-lived mesoscale convective systems. *J. Atmos. Sci.*, **47**, 3067-3077.

Raymond, D. J., C. López-Carrillo, and L. López Cavazos, 1998: Case-studies of developing east Pacific easterly waves. *Quart. J. Roy. Meteor. Soc.*, **124**, 2005-2034.

Reasor, P. D., M. T. Montgomery, F. D. Marks Jr., and J. F. Gamache, 2000: Low-wavenumber structure and evolution of the hurricane inner core observed by airborne dual-doppler rada. *Mon. Wea. Rev.*, **128**, 1653-1680.

Reasor, P. D., M. T. Montgomery, and L. D. Grasso, 2004: A new look at the problem of tropical cyclones in vertical shear flow: Vortex resiliency. *J. Atmos. Sci.*, **60**, 97-116.

Riehl, H., and J. S. Malkus, 1958: On the heat balance in the equatorial trough zone. *Geophysica*, **6**, 503-538.

Ritchie, E. A., W. M. Frank, 2007: Interactions between simulated tropical cyclones and an environment with a variable coriolis parameter. *Mon. Wea. Rev.*, **135**, 1889-1905.

Rogers, R. F., and J. M. Fritsch, 2001: Surface Cyclogenesis from Convectively Driven Amplification of Midlevel Mesoscale Convective Vortices. *Mon. Wea. Rev.*, **129**, 605-637.

Rotunno, R., and K. A. Emanuel, 1987: An Air-Sea Interaction Theory for Tropical Cyclones. Part II: Evolutionary Study Using a Nonhydrostatic Axisymmetric Numerical Model. *J. Atmos. Sci.*, **44**, 542-561.

Schecter, D. A., and D. H. E. Dubin, 1999: Vortex Motion Driven by a Background Vorticity Gradient. *Phys. Rev. Letters*, 2191-2194.

Schecter, D. A., and M. T. Montgomery, 2003: On the symmetrization rate of an intense geophysical vortex. *Dyn. Atmos. Oceans*, **37**, 55-88.

Schecter, D. A., and M. T. Montgomery, 2007: Waves in a cloudy vortex. *J. Atmos. Sci.*, **64**, 314 - 337.

Schubert, W. H., M. T. Montgomery, R. K. Taft, T. A. Guinn, S. R. Fulton, J. P. Kossin, and J. P. Edwards, 1999: Polygonal eyewalls, asymmetric eye contraction, and potential vorticity mixing in hurricanes. *J. Atmos. Sci.*, **56**, 1197-1223.

Simpson, J., J. B. Halverson, B. S. Ferrier, W. A. Petersen, R. H. Simpson, R. Blakeslee, and S. L. Durden, 1998: On the role of "hot towers" in tropical cyclone formation. *Meteor. Atmos. Phys.*, **67**, 15-35.

Smith, R. K., 1968: The surface boundary layer of a hurricane. *Tellus*, **20**, 473-484.

Smith, R. K., and W. Ulrich, 1990: An analytical theory of tropical cyclone motion using a barotropic model. *J. Atmos. Sci.*, **47**, 1973-1986.

Smith, R. K., and H. C. Weber, 1993: An extended analytic theory of tropical cyclone motion. *Quart. J. Roy. Meteor. Soc.*, **119**, 1149-1166.

Smith, R. K., 2006: Accurate determination of a balanced axisymmetric vortex. *Tellus*, **58A**, 98-103.

Trier, S. B., C. A. Davis, and W. C. Skamarock, 2000: Long-lived mesoconvective vortices and their environment. Part II: Induced thermodynamic destabilization in idealized simulations. *Mon. Wea. Rev.*, **128**, 3396-3412.

Wang Y., and G. J. Holland, 1996a: The beta drift of baroclinic vortices. Part II: Diabatic vortices. *J. Atmos. Sci.*, **53**, 3737-3756.

Wang, Y., and G. J. Holland, 1996b: The beta drift of baroclinic vortices. Part I: Adiabatic vortices. *J. Atmos. Sci.*, **53**, 411-427.

Wang, Y., 2001: An explicit simulation of tropical cyclones with a triply nested movable mesh primitive equation model: TCM3, Part I: Model description and control experiment. *Mon. Wea. Rev.*, **129**, 1370-1394.

Wang, Y., 2002a: Vortex Rossby waves in a numerical simulated tropical cyclone. Part I: Overall structure, potential vorticity, and kinetic energy budgets. *J. Atmos. Sci.*, **59**, 1213-1238.

Wang, Y., 2002b: Vortex Rossby waves in a numerical simulated tropical cyclone. Part II: The role in tropical cyclone structure and intensity changes. *J. Atmos. Sci.*, **59**, 1239-1262.

Weckwerth, T. M., 2000: The Effect of Small-Scale Moisture Variability on Thunderstorm Initiation. *Mon. Wea. Rev.*, **128**, 4017-4030.

Willoughby, H. E., H.-L. Jin, S. J. Lord, and J. M. Piotrowicz, 1984: Hurricane Structure and Evolution as Simulated by an Axisymmetric, Nonhydrostatic Numerical Model. *J. Atmos. Sci.*, **41**, 1169-1186.

Wu, L. and S. A. Braun, 2004: Effects of Environmentally Induced Asymmetries on Hurricane Intensity: A Numerical Study. *J. Atmos. Sci.*, **61**, 3065-3081.

Zhu, H., R. K. Smith and W. Ulrich, 2001: A minimal three-dimensional tropical cyclone model. *J. Atmos. Sci.*, **58**, 1924-1944.

Zhu, H., and R. K. Smith, 2002: The importance of three physical processes in a three-dimensional tropical cyclone model. *J. Atmos. Sci.*, **59**, 1825-1840.

Zhu, H., and R. K. Smith, 2003: Effects of vertical differencing in a minimal hurricane model. *Quart. J. Roy. Meteor. Soc.*, **129**, 1051-1069.

Zipser, E. J., and C. Gautier, 1978: Mesoscale events within a GATE tropical depression. *Mon. Wea. Rev.*, **106**, 789-805.

DOI: 10.1002/qj